

Inflation Model Based on Virasoro Squeezing

Kenji Ebata^{*}, So Katagiri^{*1}, Yoshiaki Matsuoka^{*}, Takaaki Sehara^{*}, and Akio Sugamoto[†]

^{*}*Nature and Environment, Faculty of Liberal Arts, The Open University of Japan, Chiba 261-8586, Japan*

[†]*Department of Physics, Graduate School of Humanities and Sciences, Ochanomizu University, 2-1-1 Otsuka, Bunkyo-ku, Tokyo 112-8610, Japan*

Abstract

We propose a novel mechanism for realizing slow-roll inflation that is fully consistent with observational data, based on conformal transformations acting exclusively on a complex scalar field—without coupling to the gravitational sector. These transformations generically produce a plateau in the inflaton potential, as guaranteed by the maximum modulus theorem, thereby naturally satisfying the slow-roll conditions.

Our framework utilizes squeezing operations generated by the Virasoro algebra without central extension, as developed in our earlier work. The resulting inflationary potentials depend on the Virasoro mode n , the power m of the original potential, and the squeezing parameter θ .

We present approximate analytical expressions at leading order for the special case $n = -2$, and perform numerical analyses for both $n = -2$ and other values of n . These reveal parameter regimes in which the predicted cosmological observables (n_s, r) align remarkably well with current CMB measurements.

1 Introduction

The question of the origin of the universe has been a subject of profound human curiosity since antiquity. While this inquiry once belonged to the realm of myth, the discovery of the cosmic microwave background (CMB) has, for the first time, rendered the origin of the universe amenable to rigorous scientific investigation.

Modern standard cosmology is based on the theory of inflation, which posits a period of rapid accelerated expansion in the early universe². This paradigm provides a natural explanation for key problems that plagued previous models, including the observed spatial flatness of the universe and the strong correlations among galaxies that reside in causally disconnected regions.

Furthermore, a key prediction of inflation—the generation of scalar and tensor perturbations that manifest as temperature anisotropies in the CMB—has been confirmed by high-precision observations, thereby greatly enhancing the credibility of the inflationary paradigm. The increasing precision of CMB measurements has now enabled a wide range of inflationary models to be quantitatively tested and discriminated[1, 2].

Among the well-known scenarios are the Starobinsky model based on R^2 gravity[4] and Linde’s chaotic inflation model[5]. These models have mutually influenced each other, giving rise to a wide variety of inflationary scenarios, including Higgs inflation[6], α -attractors[7] and string-inspired models[8, 9]. Recent reviews provide comprehensive summaries of these developments[5, 10].

In particular, the α -attractor models proposed by Kallosh and Linde[11] can be understood as extensions of the Starobinsky scenario. By constructing actions in which the gravitational and scalar sectors are coupled in a conformally invariant manner, these models can generate a family of inflationary potentials consistent with observational data. Theoretical advances and observational constraints on α -attractors have been intensively discussed in recent literature[7, 12, 13, 14].

A common feature among these models is that the inflaton potential enabling slow-roll inflation is typically constructed by design. In other words, the realization of slow-roll conditions is essentially a consequence of the deliberate choice of potential form, rather than being dictated by any underlying physical necessity.

¹So.Katagiri@gmail.com

²See [1]. See also[2]. For the theoretical background, refer to [3].

In this work, we propose a fundamentally different approach to this issue by introducing a new framework in which slow-roll inflation emerges naturally through the application of specific modes of conformal transformations to the scalar field alone. Notably, our construction does not require any special coupling to gravity, setting it apart from conventional models³.

This conformal transformation is realized via a higher-order squeezing operation, termed Virasoro squeezing[15]⁴, which is generated by the Virasoro algebra L_n without central extension, as developed in our previous work. Depending on the Virasoro mode n , the original potential $V(\phi)$, and the squeezing strength θ , the transformed potential typically develops a plateau structure in the asymptotic regime, as explained by the maximum modulus theorem in complex analysis. This plateau naturally facilitates slow-roll inflation for suitable choices of n and θ .

In particular, we provide an approximate analytical expression for the special case of $n = -2$, valid to leading order. This serves as a useful benchmark, but higher-order corrections must be treated numerically.

The novelty of our approach lies in the fact that, by postulating Virasoro squeezing of a complex scalar field in the early universe, the emergence of a slow-roll potential becomes a principle consequence of the underlying framework. While possible physical mechanisms responsible for such squeezing include vacuum condensation of the complex scalar field or geometric friction effects arising from intersecting branes, a detailed exploration of these origins is beyond the scope of this work. Accordingly, the present study focuses on whether appropriate Virasoro squeezing can reproduce the observed CMB fluctuations.

The remainder of this paper is organized as follows. In Section 2, we present the formalism of inflationary models based on Virasoro squeezing. Section 3 focuses on the special case of $n = -2$, where we derive analytical solutions and demonstrate that the predicted observables cover the full range of current experimental constraints, showing agreement with the t -model of the α -attractor scenario. In Section 4, we perform a numerical analysis for other values of n , identifying parameter regions consistent with observations. Section 5 provides approximate analytical expressions, derived via perturbative analysis, that capture the characteristic behavior of the model. Finally, Section 6 summarizes our conclusions and discusses prospects for future work.

Appendix A details the numerical algorithms used in our computations, while Appendix B provides the technical details of the perturbative analysis, and Appendix C discusses the validity range of the squeezing parameter θ in relation to observational constraints and regularity conditions.

2 Inflationary Models Based on Virasoro Squeezing

In this section, we describe Virasoro squeezing—a higher-order generalization of the squeezing transformation introduced in our previous work[15]. We explain how applying Virasoro squeezing to the potential $V(|\phi|)$ of an existing complex scalar field naturally leads to inflationary models that realize slow-roll inflation.

2.1 Virasoro Squeezing

The concept of squeezing based on the Virasoro algebra was first introduced in our previous work [15]⁵. In this framework, the n -th order squeezing is realized by applying the squeezing operator \hat{S}_n either to a quantum state $|\alpha\rangle$ or to an operator \hat{O} , as follows:

$$|\alpha'\rangle = \hat{S}_n|\alpha\rangle, \quad \hat{O}' = \hat{S}_n\hat{O}\hat{S}_n^{-1}. \quad (2.1)$$

³The scalar field in our model is not conformally coupled to gravity; only the scalar sector undergoes Virasoro squeezing, while the metric remains fixed.

⁴For subsequent developments of Virasoro squeezing and its algebraic generalizations, see [16, 17].

⁵We assume that the Virasoro squeezing occurs prior to the onset of inflation, as motivated by external modulation in the early universe (see Eq. (2.7)).

Here, \hat{S}_n in terms of the n -th Virasoro generator⁶, \hat{L}_n and a complex parameter⁷ θ , as

$$\hat{S}_n = e^{\theta \hat{L}_n}. \quad (2.2)$$

The generator \hat{L}_n , responsible for the conformal transformation, is given by

$$\hat{L}_n = \phi^{n+1} \frac{\partial}{\partial \phi}, \quad (2.3)$$

and satisfies the Virasoro algebra,

$$[\hat{L}_m, \hat{L}_n] = (m - n) \hat{L}_{m+n}, \quad (2.4)$$

where the central extension is neglected.⁸

The above construction is equally applicable in a classical context, including the analysis of cosmic inflation. Since \hat{L}_n is a generator of the following infinitesimal conformal transformation,

$$\phi \rightarrow \phi + \delta\theta \phi^{n+1}, \quad (2.5)$$

the finite conformal transformation (with a finite θ) can be written with $\hat{S}_n(\theta) = e^{\theta \hat{L}_n}$ as follows:

$$\phi' = F_n(\phi; \theta) = \hat{S}_n(\theta) \phi \hat{S}_n(\theta)^{-1}. \quad (2.6)$$

We use this expression in building an inflation model.

We note that under a conformal transformation, a wave of the form $\phi = e^{-i\omega t}$ is mapped to another wave $\phi^{n+1} = e^{-i(n+1)\omega t}$, which propagates with a frequency increased by a factor of $n + 1$. In periodic systems such as the harmonic oscillator or atomic systems, this corresponds to a reduction of the period to $T = \frac{T_0}{n+1}$ where T_0 is the original period. As a result, higher-frequency modes are introduced, leading to a squeezing phenomenon that drastically alters the shape of the Husimi distribution in phase space (see Figure 2 in Ref. [15]).

To realize such squeezing in a cosmological setting, we assume that, just before the onset of inflation, the universe undergoes strong external modulation, whereby higher oscillation modes are injected into the inflaton field through a time-dependent Hamiltonian H_{outside} . This Hamiltonian may be modeled as

$$H_{\text{outside}} = \frac{1}{2} \Omega(t) \phi^{n+2}, \quad (2.7)$$

where $\Omega(t)$ represents an external driving variable. For further details on higher-order squeezing, we refer the reader to Ref. [15].

2.2 Virasoro Squeezing Inflation Model

We consider the modulus of a complex scalar field as the inflaton, coupled to the spacetime metric $g_{\mu\nu}(x)$ via the action

$$S_\phi = \int d^4x \sqrt{-g(x)} \{g^{\mu\nu}(x) \partial_\mu \phi(x)^\dagger \partial_\nu \phi(x) - V_m(|\phi(x)|^2)\}, \quad (2.8)$$

where the potential is given by

⁶While the concept of n -th order Virasoro squeezing was originally introduced with integer n in our previous work [15], the formalism admits analytical continuation to real or complex values. In the present study, we explicitly adopt real-valued n in Sections 4 and 5 to enable flexible model building and detailed comparison with observational data.

⁷Although the squeezing parameter θ is generally defined as a complex number, in this study we restrict it to real values when constructing the inflationary model and performing numerical calculations. This restriction is imposed to ensure that the resulting potential remains real-valued, which is necessary for physical predictions. Importantly, the essential effects of the Virasoro transformation—such as the emergence of a plateau in the inflaton potential—are preserved under this real-valued restriction.

⁸The central extension may appear as a commutator anomaly, in the case when the Virasoro generators are given dynamically, in terms of the creation and annihilation operators of the system.

$$V_m(|\phi(x)|^2) = \frac{\lambda_m}{m} |\phi(x)|^m. \quad (2.9)$$

For a homogeneous and isotropic universe, the metric is given by the Friedmann–Lemaître–Robertson–Walker (FLRW) form, where $g_{00}(x) = 1$, and $g_{ij}(x) = -a(t)^2 \delta_{ij}$ with $a(t)$ denoting the scale factor of the three-dimensional space⁹. The action, after dividing by the spatial volume (while retaining the notation S_ϕ), becomes

$$S_\phi = \int dt a(t)^3 \left\{ |\dot{\phi}(t)|^2 - V(|\phi(t)|^2) \right\} = \int dt \left\{ a(t)^{-3} |\Pi(t)|^2 - a(t)^3 V(|\phi(t)|^2) \right\}, \quad (2.10)$$

where the canonically conjugate momentum is defined as $\Pi^\dagger = a(t)^3 \dot{\phi}$.

Suppose the scalar field undergoes a squeezing transformation described by a conformal mapping,

$$\phi' = F(\phi), \quad (2.11)$$

where $F(z)$ is a holomorphic function of a complex variable z . This squeezing is a type of canonical transformation that preserves the commutation (or Poisson bracket) relations:

$$\{\phi'(t), \Pi'(t)^\dagger\}_{\text{PB}} = \{\phi(t), \Pi(t)^\dagger\}_{\text{PB}} = 1, \quad \{\phi'(t)^\dagger, \Pi'(t)\}_{\text{PB}} = \{\phi(t)^\dagger, \Pi(t)\}_{\text{PB}} = 1. \quad (2.12)$$

The canonical structure can be most easily understood by analogy with quantum mechanics, where $\Pi^\dagger \propto \partial_\phi$ and $\Pi \propto \partial_\phi^\dagger$. Classically, the transformation can be generated by the function

$$W(\phi, \Pi^\dagger; \phi^\dagger, \Pi') = F(\phi) \Pi'^\dagger + F(\phi)^\dagger \Pi', \quad (2.13)$$

which yields $\phi' = \frac{\partial W}{\partial(\Pi'^\dagger)}$ and $\Pi^\dagger = \frac{\partial W}{\partial \phi}$.

Accordingly, we have

$$\phi' = F(\phi), \quad \Pi'^\dagger = F'(\phi)^{-1} \Pi^\dagger = F'(\phi)^{-1} a(t)^3 \dot{\phi}. \quad (2.14)$$

The action after the conformal transformation can thus be written in terms of the original field ϕ as,

$$S'_\phi = \int dt \left\{ a(t)^{-3} |\Pi'(t)|^2 - a(t)^3 V(|\phi'(t)|^2) \right\} = \int dt a(t)^3 \left\{ \frac{|\dot{\phi}|^2}{|F'(\phi)|^2} - V(|F(\phi)|^2) \right\}. \quad (2.15)$$

Next, we introduce a new scalar field $\chi(t)$, defined so that the kinetic term becomes canonical. Specifically, we set

$$\dot{\chi} = \frac{\dot{\phi}}{F'(\phi)}, \quad (2.16)$$

which determines χ as a function of ϕ via

$$\chi(\phi) = \int_0^\phi \frac{d\phi}{F'(\phi)}. \quad (2.17)$$

We assume that ϕ can be inverted to give $\phi = \phi(\chi)$. (We note that there is a phase ambiguity in the definition of χ (2.16), which may be fixed as required.)

The conformally transformed action can then be expressed in terms of χ as

$$S'_\chi = S'_\phi = \int dt a(t)^3 \left\{ |\dot{\chi}(t)|^2 - V_\chi(\chi) \right\}, \quad (2.18)$$

⁹As is customary in many inflationary scenarios including α -attractors and the Starobinsky model, we adopt a fixed FLRW background throughout, ignoring back-reaction effects.

where the new potential, denoted as $V_\chi(\chi)$, is related to the original potential by

$$V_\chi(\chi) = V(|F(\phi(\chi))|^2). \quad (2.19)$$

To construct a Virasoro-based inflation model, it is necessary to explicitly specify the conformal transformation $F_n(\phi, \theta)$, which corresponds to the n -th Virasoro squeezing with finite parameter θ . This transformation is defined by¹⁰

$$\phi' = F_n(\phi; \theta) \equiv \phi_n(\theta) = \hat{S}_n(\theta)\phi\hat{S}_n(\theta)^{-1}. \quad (2.20)$$

Differentiating both sides of this equation with respect to θ yields

$$\frac{d\phi_n(\theta)}{d\theta} = [\hat{L}_n, \phi_n(\theta)] = \phi_n(\theta)^{n+1}, \quad (2.21)$$

where we have used $\hat{L}_n = \hat{S}_n(\theta)\hat{L}_n\hat{S}_n(\theta)^{-1} = \hat{L}_n(\theta)$.

Solving this differential equation, as introduced in Subsection 2.1, we obtain:

$$F_n(\phi; \theta) = \phi_n(\theta) = \frac{\phi}{(1 - n\theta\phi^n)^{1/n}}. \quad (2.22)$$

This allows us to construct a family of inflationary models parameterized by the Virasoro mode n :

$$S'^{(n)} = \int dt a(t)^3 \left\{ |\dot{\chi}_n(t)|^2 - V_\chi^{(n)}(\chi_n) \right\}. \quad (2.23)$$

We focus on the case where the original potential takes the form $|\phi|^m$,

$$V_\chi^{(m,n)}(\chi_n) = \frac{\lambda_m}{m} |F_n(\phi(\chi_n); \theta)|^m, \quad (2.24)$$

where $\phi(\chi_n)$ is the inverse function of $\chi_n(\phi)$, defined as

$$\chi_n(\phi) = \int_0^\phi d\phi \left(\frac{dF_n(\phi; \theta)}{d\phi} \right)^{-1} = \int_0^\phi d\phi (1 - n\theta\phi^n)^{1+1/n}. \quad (2.25)$$

2.3 Asymptotic Behavior and Plateau Formation in n -th Virasoro Inflation

In this subsection, we examine how n -th order Virasoro squeezing leads to the formation of plateau structures in the inflaton potential, depending on the strength of squeezing.

A key observation is that, as dictated by the maximum modulus theorem, the potential after Virasoro squeezing achieves its maximal value at the boundary of its domain. Specifically, the transformed potential $V(|F_n(\phi(\chi_n); \theta)|)$ attains its maximum in the asymptotic limit. We will demonstrate how, depending on the value of the Virasoro index n , the inflaton potential can indeed develop a plateau at infinity.

Depending on the value of n , the resulting inflaton potentials fall into different asymptotic classes. In particular, the cases $n > 0$, $n < -2$ and $n = 0, -1, -2$ exhibit distinct structures.

In this subsection, we analyze the asymptotic behavior of the inflaton potential $V(\chi_n)$ induced by Virasoro transformations with various indices n . The resulting potential may exhibit features such as plateau structures or power-law growth, each having significant implications for the inflationary dynamics. We classify the models into physically meaningful categories and focus on the cases $n > 0$, which yield viable inflationary scenarios, and $n = -2$, which permits analytical treatment.

¹⁰The same analysis can be done for the momentum Π [15].

2.3.1 Special Case: $n = -2$

We now examine the special case of $n = -2$ which allows for an approximate analytical representation of the transformation and the potential at leading order.

For $n = -2$, the conformal transformation takes the form

$$F_{-2}(\phi; \theta) = \pm \sqrt{\phi^2 + 2\theta}. \quad (2.26)$$

Accordingly, the canonical field χ_{-2} is given by

$$\pm \chi_{-2} = \int^\phi \frac{d\phi}{\phi} \sqrt{\phi^2 + 2\theta} = \sqrt{\phi^2 + 2\theta} - \sqrt{2\theta} \tanh^{-1} \sqrt{\frac{\phi^2 + 2\theta}{2\theta}}. \quad (2.27)$$

Note that the integration constant can shift χ_{-2} . Therefore, without loss of generality, we omit the \pm signs in what follows and treat F_{-2} and χ_{-2} as real-valued functions.

The above relation leads to

$$\tanh \left(\frac{F_{-2}(\phi; \theta)}{\sqrt{2\theta}} - \frac{\chi_{-2}}{\sqrt{2\theta}} \right) = \frac{F_{-2}(\phi; \theta)}{\sqrt{2\theta}}. \quad (2.28)$$

In the case of $\theta < 0$, replacing $[\tanh \rightarrow \tan]$ and setting $\theta = -|\theta|$, we obtain

$$\tan \left(\frac{F_{-2}(\phi; -|\theta|)}{\sqrt{2|\theta|}} - \frac{\chi_{-2}}{\sqrt{2|\theta|}} \right) = \frac{F_{-2}(\phi; -|\theta|)}{\sqrt{2|\theta|}}. \quad (2.29)$$

Coming back to the case of $\theta > 0$, we find the following approximate behavior:

$$F_{-2}(\phi; \theta) \sim \begin{cases} -\sqrt{2\theta}, & \text{for } \chi_{-2} \gg \sqrt{2\theta}, \\ 0, & \text{for } |\chi_{-2}| \ll \sqrt{2\theta}, \end{cases} \quad (2.30)$$

we find the asymptotic behavior

$$V_\chi^{(m, -2)}(\chi_{-2}) = \frac{\lambda_m}{m} |F_{-2}(\chi_{-2})|^m \quad (2.31)$$

$$\sim \frac{\lambda_m}{m} \begin{cases} |2\theta|^{m/2} \text{ (giving plateau)} & \text{for } |\chi_{-2}| \gg |\sqrt{2\theta}|, \\ 0, & \text{for } |\chi_{-2}| \ll |\sqrt{2\theta}|. \end{cases} \quad (2.32)$$

In contrast, for $\theta < 0$, the behavior becomes

$$F_{-2}(\phi; \theta) \sim \begin{cases} \chi_{-2}, & \text{for } \chi_{-2} \gg \sqrt{2|\theta|}, \\ \frac{\pi}{2} \sqrt{2|\theta|}, & \text{for } |\chi_{-2}| \ll \sqrt{2|\theta|}. \end{cases} \quad (2.33)$$

The corresponding inflaton potential for $\theta < 0$ is asymptotically

$$V_\chi^{(m, -2)}(\chi_{-2})(\theta < 0) = \frac{\lambda_m}{m} |\chi_{-2}|^m \text{ for } |\chi_{-2}| \gg |\sqrt{2\theta}|, \quad (2.34)$$

which resembles the original unsqueezed potential and is therefore not of particular interest.

It is characteristic and interesting that for $\theta > 0$, the potential exhibits a plateau in the limit $|\chi_{-2}| \gg |\sqrt{2\theta}|$, making it a viable inflationary scenario.

The analytical properties of the potential in this case allow for a detailed discussion, which will be presented in Section 3.

2.3.2 Model with $n > 0$

From the definition of the inflaton field χ_n in (2.25),

$$\chi_n(\phi) = \int_0^\phi d\phi (1 - n\theta\phi^n)^{1+1/n}, \quad (2.35)$$

we observe that for $n > 0$, the integral is dominated by large values of $|\phi|$, leading to the approximation

$$\chi_n \approx \frac{(-n\theta)^{1+1/n}}{n+2} \phi^{n+2} \text{ for } n > 0. \quad (2.36)$$

Furthermore, according to the maximum modulus theorem in complex analysis, it is naturally understood that the modulus of the potential gives a plateau (maximum) at $|\phi| \rightarrow \infty$,

$$|V_m(|\phi|^2)| = \frac{\lambda_m}{m} \left| \frac{\phi}{(1 - n\theta\phi^n)^{1/n}} \right|^m \rightarrow \frac{\lambda_m}{m} |n\theta|^{-1/n}, \text{ (plateau) for } |\phi| \rightarrow \infty. \quad (2.37)$$

Since $|\phi| \rightarrow \infty$ corresponds to $|\chi_n| \rightarrow \infty$ for $n > 0$, and χ_n and ϕ are related in a power-law fashion, the new potential $V_\chi^{(m,n)}(\chi_n)$ also develops a plateau at $|\chi_n| = \infty$, from which the inflaton field χ_n rolls down slowly. This naturally leads to viable slow-roll inflation scenarios.

More explicitly, the leading-order relation between ϕ and χ_n is given by

$$\phi \approx A_n \chi_n^{\frac{1}{n+2}}, \quad (2.38)$$

where we have introduced

$$A_n \equiv \left(\frac{n+2}{(-n\theta)^{1+1/n}} \right)^{\frac{1}{n+2}}. \quad (2.39)$$

Therefore, the inflaton potential for $n > 0$, can be approximated by,

$$V_\chi^{(m,n)}(\chi_n) \approx \frac{\lambda_m}{m} \left| \frac{A_n \chi_n^{\frac{1}{n+2}}}{\left(1 - n\theta(A_n)^n \chi_n^{\frac{n}{n+2}}\right)^{1/n}} \right|^m. \quad (2.40)$$

Interestingly, the inflaton potential $V_\chi^{(m,n)}(\chi_n)$ for $n < -2$ takes the same formal expression as that for $n > 0$; the only difference is n is negative, i.e., $n = -|n|$. However, the asymptotic behavior differs, as the plateau emerges in the opposite limit $\phi \rightarrow 0$ rather than $\phi \rightarrow \infty$.

On the other hand, $n = 0$ and $n = -1$ correspond to trivial transformations¹¹ of the potential and are therefore not considered further.

The numerical and approximate analytical results for the case $n > 0$ will be discussed in detail in Section 4.

2.4 Analytical Origin of the Plateau via the Maximum Modulus Theorem

In this section, we provide a complex analysis perspective to explain why n -th order Virasoro squeezing generates plateau-like potentials, as discussed in the previous section.

The mathematical underpinning of this phenomenon is the classical maximum modulus theorem in complex analysis[18]. We summarize the theorem below.

¹¹These correspond to special cases of the squeezing transformation that act trivially on the potential:

$F_0(\phi) = e^\theta \phi$ corresponds to a simple rescaling, and

$F_1(\phi) = \phi + \theta$ corresponds to a constant shift.

Neither of these alters the essential shape of the potential, and they are therefore not considered further.

Proposition. *Maximum Modulus Theorem*

Let $f(z)$ be a holomorphic (analytic) and non-constant function inside and on a closed curve C . Then, the modulus $|f(z)|$ does not attain its maximum value anywhere in the interior of C .

This result can be proven using Cauchy's integral theorem and the triangle inequality. From this theorem, the following corollary immediately follows.

Corollary. *The maximum of $|f(z)|$ is always attained on the boundary C . That is, by the maximum modulus theorem, $|f(z)|$ cannot have a maximum in the interior of C . However, by the Weierstrass theorem, any continuous function must attain its maximum somewhere, and therefore the maximum must occur on the boundary C .*

Therefore, the maximum value of a holomorphic function always appears on the boundary of its domain. When the potential is expressed as a transformation of a holomorphic function, its asymptotic behavior—i.e., its value at the boundary—becomes dominant. This underlies the emergence of plateau-like structures in the transformed inflaton potential.

Furthermore, by the Cauchy integral formula (Goursat's theorem), the first derivative of $f(z)$ at $z = a$ can be written as

$$f^1(a) = \frac{1}{2\pi i} \oint_C \frac{f(z)}{(z-a)^2} dz. \quad (2.41)$$

Letting $z - a = re^{i\theta}$, we obtain the inequality

$$|f^1(a)| \leq \frac{1}{2\pi r} \int_0^{2\pi} |f(a + re^{i\theta})| d\theta. \quad (2.42)$$

If we assume the boundary is at infinity and that the boundary value of $f(z)$ satisfies $\lim_{|z| \rightarrow \infty} f(z) = f_\infty$ (a finite value), then

$$\lim_{|z| \rightarrow \infty} |f^1(z)| \leq \frac{1}{r} |f_\infty|. \quad (2.43)$$

Thus, if $f_\infty = 0$, the derivative vanishes asymptotically and a plateau is formed.

2.4.1 Plateau Formation via Virasoro Squeezing

The Virasoro squeezing transformation is given by

$$F_n(\phi; \theta) = \frac{\phi}{(1 - n\theta\phi^n)^{1/n}}. \quad (2.44)$$

In the limit where ϕ becomes large, the transformation asymptotically approaches

$$F_n(\phi; \theta) \approx \frac{1}{(-)^{1/n} n^{1/n} \theta^{1/n}}. \quad (2.45)$$

The potential after transformation takes the form

$$V_m(|F_n(\phi; \theta)|) = \frac{\lambda}{m} \left(\frac{\phi}{(1 - n\theta\phi^n)^{1/n}} \right)^m. \quad (2.46)$$

For $n > 0$, if θ is sufficiently large and positive, $F_n(\phi; \theta)$ approaches zero in the large- ϕ limit. For $n < 0$, if θ is sufficiently close to zero, $F_n(\phi; \theta)$ also tends toward zero. In both cases, this asymptotic behavior leads to the formation of a plateau in the potential.

Analysis in the χ Representation

In the χ representation, the relationship between ϕ and χ_n can be approximated as

$$\phi(\chi_n) \approx A_n \chi_n^{1/(n+2)} \quad (2.47)$$

where A_n is a constant determined by the transformation.

For $n > -2$, both χ and ϕ become large in the asymptotic regime, and as a result, $F_n(\phi, \theta)$ forms a plateau at large field values. Conversely, for $n < -2$, the limit $\chi_n \rightarrow 0$ corresponds to $\phi \rightarrow \infty$, so $F_n(\phi, \theta)$ develops a plateau in the vicinity of $\chi_n \rightarrow 0$.

Thus, the asymptotic behavior of the potential in our model can be understood as a generic feature of holomorphic transformations, as established by complex analysis.

3 The $n = -2$ Virasoro Squeezed model

In this section, we analyze the case of $n = -2$ which admits an approximate analytical treatment at leading order. We show that, to leading order, the resulting potential acquires a hyperbolic tangent (tanh) form, which reproduces the well-known Starobinsky potential—or, equivalently, the t -model potential in the α -attractor class.

Crucially, these results are obtained by applying $n = -2$ Virasoro squeezing to a potential of the form $V = \frac{\lambda}{m} |\phi|^m$, without introducing any special coupling to gravity. We also demonstrate that, at higher orders of approximation, the $n = -2$ model exhibits deviations from the t -model potential.

Near the plateau, in the limit $|\chi_{-2}| \approx \infty$, the relation between F_{-2} and χ_{-2} can be approximated. From the defining relation (see (2.28)), we use the following approximation

$$F_{-2}(\phi; \theta) = \sqrt{2\theta} \tanh\left(\frac{F_{-2}(\phi; \theta)}{\sqrt{2\theta}} - \frac{\chi_{-2}}{\sqrt{2\theta}}\right) \approx \varepsilon \sqrt{2\theta} \tanh\left(-\frac{1}{\sqrt{2\theta}} |\chi_{-2}|\right), \quad \varepsilon = \chi_2/|\chi_{-2}|, \quad (3.1)$$

where we have set $\varepsilon = 1$ without loss of generality.

This leads to

$$V_{\chi,0}^{(-2)} = V_{\chi}^{(-2)}(\sqrt{2\theta} \tanh\left(-\frac{1}{\sqrt{2\theta}} |\chi_{-2}|\right)) \approx V_{\chi}^{(-2)}\left(-\sqrt{2\theta} \left(1 - 2e^{-\frac{2|\chi_{-2}|}{\sqrt{2\theta}}}\right)\right). \quad (3.2)$$

It should be emphasized that the original potential $V_{\chi}^{(-2)}(\phi)$ before squeezing can be arbitrary; thus, the Starobinsky-type and α -attractor-type t -models emerge as lowest-order approximations within this framework.

Incorporating the next-order correction, we set

$$F_{-2} = -\sqrt{2\theta} \tanh\left(\frac{\chi_{-2}}{\sqrt{2\theta}}\right) + \Delta F_{-2}. \quad (3.3)$$

Substituting this expression and expanding to leading order, we obtain

$$-\sqrt{2\theta} \tanh\left(\frac{\chi_{-2}}{\sqrt{2\theta}}\right) + \Delta F_{-2} \approx -\sqrt{2\theta} \tanh\left(\frac{\chi_{-2}}{\sqrt{2\theta}}\right) - \left(1 - \tanh^2 \frac{\chi_{-2}}{\sqrt{2\theta}}\right) \left(1 + \frac{1}{\sqrt{2\theta}} \Delta F_{-2}\right). \quad (3.4)$$

Solving for ΔF_{-2} , we find

$$\Delta F_{-2} = -\frac{2\sqrt{2\theta}}{3 + \cosh\left[2\frac{\chi_{-2}}{\sqrt{2\theta}}\right]}. \quad (3.5)$$

Thus, the corrected expression for F_{-2} is

$$F_{-2} \approx -\sqrt{2\theta} \tanh\left(\frac{\chi_{-2}}{\sqrt{2\theta}}\right) - \frac{2\sqrt{2\theta}}{3 + \cosh\left[2\frac{\chi_{-2}}{\sqrt{2\theta}}\right]}. \quad (3.6)$$

Accordingly, the inflaton potential becomes

$$V_{\chi} = V_{\chi}^{(-2)}\left(\sqrt{2\theta} \tanh\left(-\frac{1}{\sqrt{2\theta}} |\chi_{-2}|\right) - \frac{2\sqrt{2\theta}}{3 + \cosh\left[2\frac{\chi_{-2}}{\sqrt{2\theta}}\right]}\right). \quad (3.7)$$

This shows that the $n = -2$ model introduces corrections to the α -attractor t -model potential at higher orders of approximation.

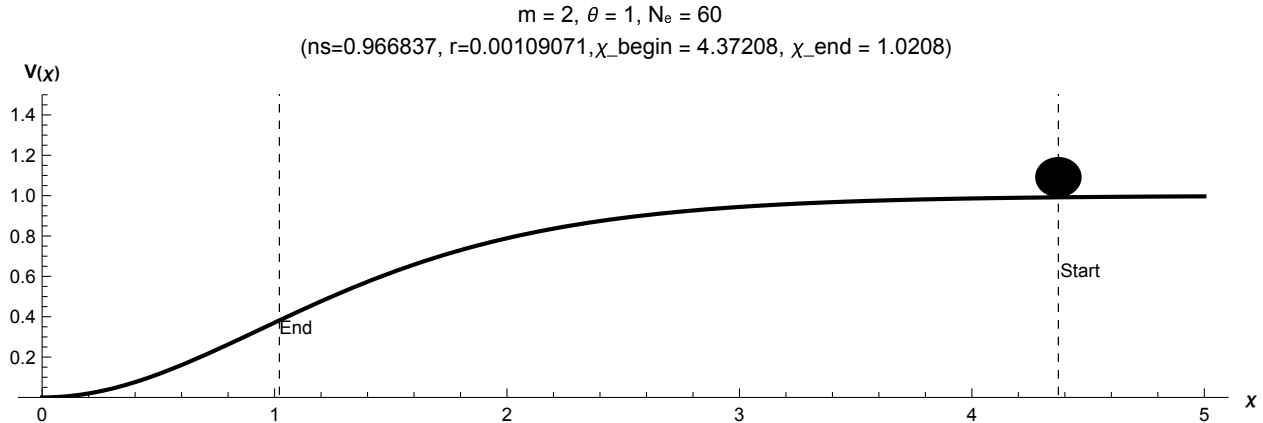


Figure 3.1: Potential $V(\chi)$ for $n = -2, m = 2, \theta = 1$. The horizontal axis represents the inflaton field χ , and the vertical axis shows the potential $V(\chi)$. The vertical dashed lines indicate the beginning and end points of the slow-roll inflation phase.

For a potential of the form $V^{(m)} = \frac{\lambda_m}{m!} \phi^m$, the inflaton potential is approximately given by

$$V_\chi^{(m,-2)} = \frac{\lambda_m}{m!} \varepsilon^m \left(\sqrt{2\theta} \right)^m \left(\tanh \left(-\frac{1}{\sqrt{2\theta}} |\chi_{-2}| \right) + O(\Delta F_{-2}) \right)^m. \quad (3.8)$$

The slow-roll parameters are computed numerically¹². For example, setting $m = 2, \theta = 1$, and $N_e = 60$, we obtain $n_s = 0.966837$ and $r = 0.00109071$, which are within the Planck observational constraints[1, 2].

Figure 3.1 shows the potential for $n = -2, m = 2$, and $\theta = 1$, along with the starting and ending points of the slow-roll phase and the evolution of the inflaton field.

Figure 3.2 illustrates the behavior of (n_s, r) in the parameter space $\theta = 0 \sim 100$ for $N_e = 50, 55, 60$. The gray shaded region indicates the range allowed by current observational constraints. These results demonstrate that the full range of observed values can be covered by adjusting the e-folding number. Figure 3.3 shows the behavior of (n_s, r) for varying $m = 2, 4, 8$, again as a function of θ in the range $0 \sim 100$. As m increases, the vertical trajectories tilt diagonally, while still remaining consistent with observational bounds.

While the leading-order behavior of the potential can be captured analytically, a precise evaluation of the slow-roll parameters n_s and r requires numerical computation. Therefore, numerical analysis is essential for fully assessing the model's viability.

These results confirm that, in the $n = -2$ Virasoro squeezed model, the inflaton potential reproduces the essential features of the Starobinsky and α -attractor t -model potentials at leading order, while allowing for characteristic corrections at higher orders. In the next section, we generalize our analysis to other values of n and examine the resulting phenomenology through numerical calculations.

4 Numerical Results and Discussion

Although the case $n = -2$ admits an analytic expression for the conformal transformation, the evaluation of the slow-roll parameters n_s and r relies on the approximate expression (3.1) and its numerical integration. This semi-analytic treatment was already presented in Section 3.

We now turn to other values of n , for which no closed-form expression is available for the transformation $F_n(\phi; \theta)$, and a fully numerical approach is required.

As discussed in Section 3, the inflationary potential generated by Virasoro squeezing satisfies the slow-roll conditions. To obtain precise predictions for the observables n_s and r , we now adopt a numerical approach.

¹²The use of slow-roll parameters (n_s, r) as effective indicators of quantum fluctuations in both scalar and metric perturbations follows standard cosmological practice (e.g., Planck Collaboration [1]).

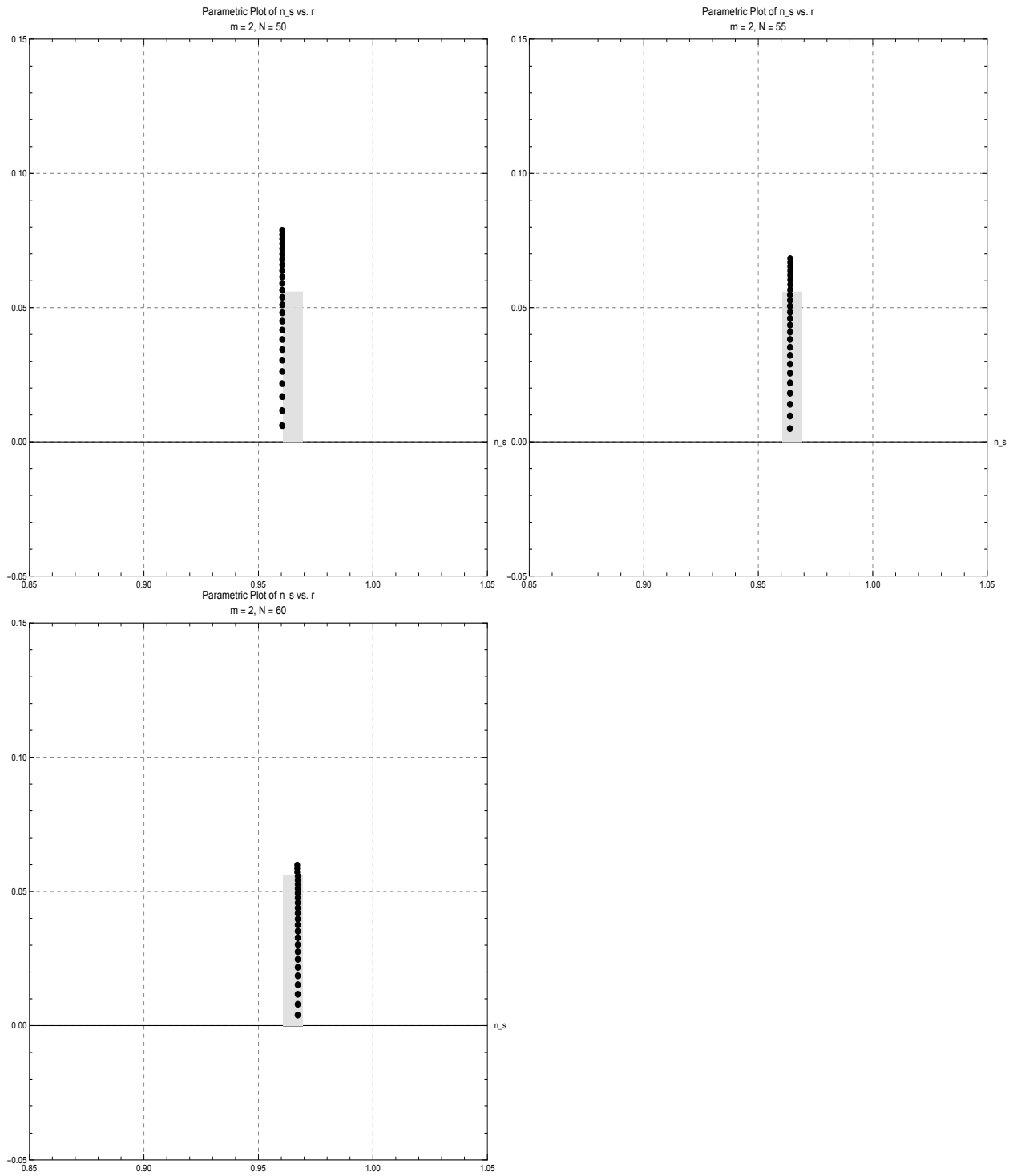


Figure 3.2: (n_s, r) parametric plot with $\theta = 0 \sim 100$, $n = -2$, $m = 2$, $N_e = 50, 55, 60$. The gray shaded region indicates the range allowed by current observational constraints.

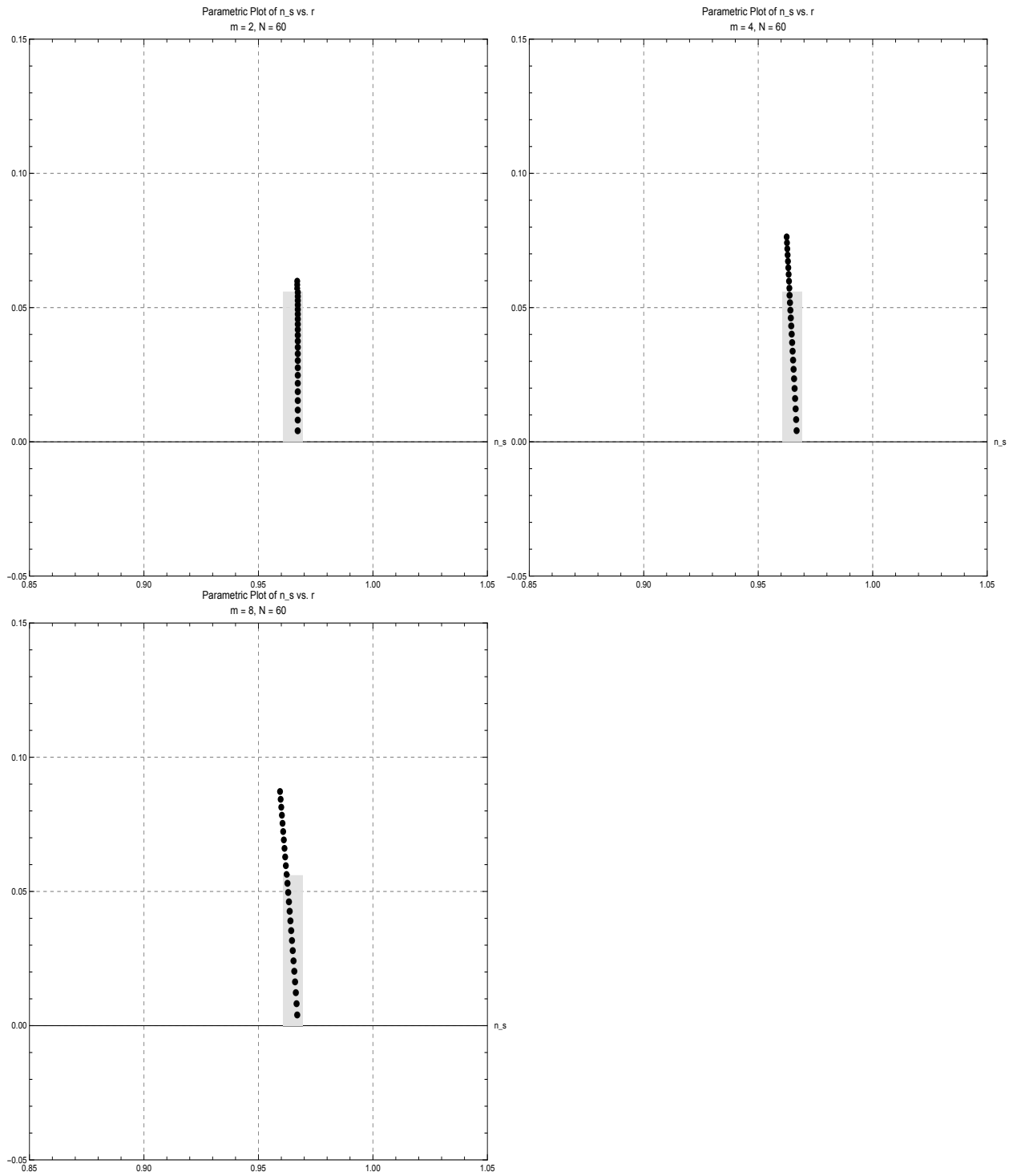


Figure 3.3: (n_s, r) parametric plot with $\theta = 0 \sim 100$, $n = -2$, $m = 2, 4, 8$, $N_e = 60$. The gray shaded region indicates the range allowed by current observational constraints.

We describe the computational setup and algorithm, and compare the resulting predictions with observational constraints. For convenience, we define the transformed field variable $y \equiv F_n(\phi)$, which will be used in the following analysis.

Unlike the approximate analysis in Section 3, we here rely entirely on numerical methods. Instead of using the standard e-folding expression involving V/V' , we determine the endpoint y_e by solving $\epsilon_V(y_e) = 1$, and then obtain the initial value y_b by integrating the e-folding number numerically. The slow-roll parameter ϵ_V and η_V at y_b are then used to compute n_s and r ¹³.

This approach enables us to systematically treat the different branches of the Virasoro transformation, including nontrivial root structures, and to explore regions of parameter space that are inaccessible to analytical approximations.

4.1 Numerical Setup

The technical details of our numerical procedure are given in Appendix A. Here, we briefly outline the main computational setup, with particular emphasis on the treatment of the branch structures that arise from the Virasoro-generated conformal transformations.

The transformation $\phi \rightarrow F_n(\phi; \theta)$ involves fractional powers (i.e., n -th roots), and the evaluation of these roots depends on the proper choice of complex branch¹⁴. In our analysis, we define and classify three representative branches according to the sign of the Virasoro index n and the manner in which the root is taken:

- [Branch1+] (for $n > 0$)

This branch corresponds to choosing a non-principal branch of the n -th root for the transformation variable. It was introduced to investigate the behavior near singular limits, such as $\theta \rightarrow 0$.

- [Branch2+](for $n > 0$)

In this standard branch, the principal n -th root is adopted. This leads to well-behaved potentials and is considered the most physically natural choice for $n > 0$.

- [Branch3-](for $n < 0$)

In this case, the transformation involves an $|n|$ -th root rather than an n -th root. With the variable change $t = \frac{1}{|n\theta|} \phi^{|n|}$, the transformation is given by $y = F(\phi) = (t + \text{sign}(\theta))^{1/|n|}$.

Among these, Branch 2+ and, in some cases, Branch 1+ yield potentials that exhibit plateau-like behavior after transformation. As a result, these branches naturally satisfy the slow-roll conditions and provide viable predictions for the spectral index n_s and the tensor-to-scalar ratio r within certain regions of parameter space. Also, Branch 3– does yield valid parameter sets that are consistent with observational bounds within the scanned range for $n = -2$ which is match for Analytical case.

Therefore, in the following subsections, we focus primarily on Branch 2+ and Branch 1+ and Branch 3- in our numerical analysis.

4.2 Numerical Results

We performed a parameter scan for each branch, exploring $n = +1 \sim +6$ (and $n = -1 \sim -6$ for Branch 3), $m = -16 \sim +16$ and $\theta \in [-10^7, 10^{-2}] \cup [10^{-2}, 10^7]$, in order to identify combinations of (n, m) that yield predictions consistent with observational bounds. Representative results for each branch are summarized in Table 1 and Table 2, respectively. For each branch, we list the Virasoro index n , the potential power m , the minimum and maximum values of $\theta(\theta_{\min}, \theta_{\max})$ for which the predictions agree with observational constraints, as well as the resulting spectral index n_s and tensor-to-scalar ratio r , together with their corresponding

¹³Definitions of the slow-roll parameters ϵ_V and η_V are provided in Appendix A.

¹⁴Strictly speaking, the conformally transformed field $F_n(\phi)$ and its canonically normalized counterpart χ_n are multivalued complex functions. A fully consistent treatment would require formulating slow-roll inflation as a multi-component field theory, where the inflaton trajectory follows a curved path in field space. This introduces significant complications in analyzing the dynamics and evaluating the potential. In this work, we simplify the analysis by restricting to real-valued field configurations and explicitly accounting for branch structures arising from root ambiguities. A more complete treatment that incorporates complex inflaton trajectories[19] is left for future investigation.

n	m	θ_{\min}	θ_{\max}	n_s	σ_{n_s}	r	σ_r
4	0.5	-0.000116861	0.000116861	0.96885	0.00013	0.01248	0.00191
4	1	-0.000054556	0.000054556	0.96771	0.00062	0.02818	0.00874
4	2	-0.000027295	0.000027295	0.96635	0.00158	0.03658	0.00889
4	3	-0.000019307	0.000019307	0.96651	0.00153	0.04143	0.00730
4	4	-0.000016810	0.000016810	0.96718	0.00132	0.04368	0.00612
4	5	-0.000014636	0.000014636	0.96740	0.00108	0.04724	0.00506
4	6	-0.000013656	0.000013656	0.96788	0.00075	0.04893	0.00357
4	7	-0.000013656	0.000013656	0.96813	0.00057	0.05109	0.00281
4	8	-0.000013656	0.000013656	0.96846	0.00039	0.05235	0.00197
4	9	-0.000013656	0.000013656	0.96868	0.00025	0.05375	0.00129
4	10	-0.000014636	0.000014636	0.96891	0.00015	0.05470	0.00079

Table 1: Representative parameter sets for Branch 1. Listed are the Virasoro index n , the potential power m , the allowed range of the squeezing parameter θ , the predicted values of the spectral index n_s and tensor-to-scalar ratio r , and their respective standard deviations. The standard deviations (σ_{n_s}, σ_r) are computed over all valid values of θ that satisfy the observational constraints for each (n, m) pair.

uncertainties (σ_{n_s}, σ_r). For each pair (n, m) , the standard deviations σ_{n_s} and σ_r are computed from all solutions obtained by scanning over a range of values of the squeezing parameter θ , including cases where multiple valid solutions exist for the same θ . These values quantify the predictive variation of the model under parameter scanning and should not be interpreted as observational uncertainties.

The numerical results for Branch 3 are consistently the observationally allowed region for $n = -2$. This result is confirmed by the data presented in Table 3.

We find that the results for $n = -2$ show excellent agreement with those obtained from the approximate analytical treatment (e.g., $n_s = 0.966837, r \simeq 0.00109071$ for $\theta \sim 1$).

A comprehensive summary of the results is provided in Table 4. Branch 1, Branch 2 and Branch 3 all yield solutions that are consistent with observational bounds over a wide range of n and m , and in particular, r .

It is also observed that larger values of n tend to satisfy the observational bounds with smaller values of θ , and that smaller values of m are effective in realizing lower values of r .

Figures 4.1 and 4.2 show parametric plots in the (n_s, r) plane for various combinations (n, m) based on the numerical data described above. In these plots, the parameter θ is varied, and the predicted values trace a trajectory from high n_s and low r to lower n_s and higher r within the region allowed by current observations.

It should be noted, however, that as θ changes, some parameter combinations may leave the allowed region, resulting in predictions that fall outside the observational constraints.

In summary, our numerical analysis demonstrates that Branch 1, Branch 2 and Branch 3 can all realize slow-roll inflation with predictions for (n_s, r) consistent with current observational constraints over a broad range of model parameters. Notably, the ability to achieve small values of r without fine-tuning is a distinctive feature of this framework. At the same time, the results highlight the sensitivity of the predictions to the choice of the Virasoro index n , the potential power m , and the squeezing parameter θ , with some parameter combinations falling outside the observationally allowed region. In particular, the value of $r \lesssim 0.03$ achieved in Branch 3 is noteworthy. This value is not excluded by the results of Planck PR4 + BK18.

In order to perform more accurate calculations beyond the branched point, it is necessary to consider inflation as a complex scalar field. In this case, contributions from the curvature of the inflaton beyond the horizon also come into play, and complex corrections are added to the slow-roll parameter. These accurate calculations will improve the predictive power of the theory[19].

These findings suggest that Virasoro-squeezed inflation models provide a flexible and unifying framework for inflationary phenomenology. Further studies, including more systematic exploration of the parameter space and direct comparison with upcoming cosmological observations, would be valuable for assessing the full predictive power and testability of the model.

n	m	θ_{\min}	θ_{\max}	n_s	σ_{n_s}	r	σ_r
3	2	-0.000165213	-0.000067153	0.96807	0.00065	0.04588	0.00530
3	3	-0.000189756	-0.000101746	0.96816	0.00060	0.04880	0.00363
3	4	-0.000203362	-0.000143845	0.96850	0.00041	0.05120	0.00231
3	5	-0.000217944	-0.000189756	0.96872	0.00020	0.05386	0.00111
4	0.5	-0.000116861	-0.000033598	0.96885	0.00013	0.01248	0.00193
4	1	-0.000054556	-0.000002777	0.96771	0.00063	0.02818	0.00877
4	2	-0.000027295	-0.000002976	0.96635	0.00159	0.03658	0.00893
4	3	-0.000019307	-0.000003664	0.96651	0.00154	0.04143	0.00734
4	4	-0.000016810	-0.000004510	0.96718	0.00133	0.04368	0.00616
4	5	-0.000014636	-0.000005179	0.96740	0.00109	0.04724	0.00511
4	6	-0.000013656	-0.000006375	0.96788	0.00075	0.04893	0.00361
4	7	-0.000013656	-0.000007323	0.96813	0.00058	0.05109	0.00284
4	8	-0.000013656	-0.000009013	0.96846	0.00039	0.05235	0.00200
4	9	-0.000013656	-0.000010352	0.96868	0.00025	0.05375	0.00133
4	10	-0.000014636	-0.000012743	0.96891	0.00015	0.05470	0.00083
5	0.5	-0.000067153	-0.000001297	0.96675	0.00118	0.01251	0.00530
5	1	-0.000015685	-0.000000107	0.96603	0.00175	0.02598	0.01371
5	2	-0.000004208	-0.000000186	0.96479	0.00253	0.02995	0.00978
5	3	-0.000002105	-0.000000162	0.96543	0.00248	0.03414	0.00928
5	4	-0.000001489	-0.000000152	0.96582	0.00216	0.03826	0.00816
5	5	-0.000001053	-0.000000162	0.96613	0.00175	0.04189	0.00685
5	6	-0.000000917	-0.000000174	0.96667	0.00156	0.04396	0.00632
5	7	-0.000000745	-0.000000186	0.96699	0.00128	0.04631	0.00538
5	8	-0.000000695	-0.000000214	0.96766	0.00095	0.04666	0.00412
5	9	-0.000000649	-0.000000230	0.96774	0.00081	0.04916	0.00364
5	10	-0.000000605	-0.000000264	0.96796	0.00069	0.05071	0.00321
5	11	-0.000000605	-0.000000303	0.96833	0.00053	0.05122	0.00257
5	12	-0.000000565	-0.000000348	0.96843	0.00037	0.05278	0.00184
5	13	-0.000000565	-0.000000399	0.96857	0.00029	0.05388	0.00148
5	14	-0.000000605	-0.000000459	0.96871	0.00020	0.05476	0.00105
5	15	-0.000000605	-0.000000565	0.96896	0.00008	0.05489	0.00043
5	16	-0.000000649	-0.000000649	0.96906	0.00000	0.05563	0.00000
6	0.5	-0.000025469	-0.000000100	0.96452	0.00215	0.01126	0.00614
6	1	-0.000003664	-0.000000115	0.96511	0.00268	0.01198	0.00459
6	2	-0.000000605	-0.000000100	0.96678	0.00142	0.01607	0.00260
6	3	-0.000000246	-0.000000100	0.96798	0.00067	0.01916	0.00142
6	4	-0.000000132	-0.000000100	0.96870	0.00024	0.02196	0.00058

Table 2: Same as Table 1, but for Branch 2.

n	m	θ_{\min}	θ_{\max}	n_s	σ_{n_s}	r	σ_r
-2	-16	1.252403755	9.330927435	0.96309	0.00193	0.00720	0.00395
-2	-15	0.771290612	8.124084578	0.96379	0.00202	0.00550	0.00370
-2	-14	0.949387718	5.746434969	0.96399	0.00178	0.00482	0.00220
-2	-13	0.719685673	5.003202954	0.96461	0.00168	0.00392	0.00211
-2	-12	0.949387718	5.003202954	0.96472	0.00141	0.00357	0.00200
-2	-11	0.885866790	4.064644396	0.96485	0.00126	0.00300	0.00134
-2	-10	0.335981829	3.538931695	0.96430	0.00107	0.00303	0.00131
-2	-9	1.438449888	2.875058041	0.96435	0.00067	0.00292	0.00067
-2	-8	0.584678728	2.335721469	0.96471	0.00077	0.00218	0.00064
-2	-7	0.335981829	1.652133406	0.96579	0.00045	0.00142	0.00061
-2	-6	0.272954479	1.252403755	0.96547	0.00064	0.00107	0.00044
-2	-5	0.021052723	0.885866790	0.96592	0.00055	0.00068	0.00034
-2	-4	0.360073348	0.360073348	0.96624	0.00000	0.00041	0.00000
-2	-3	0.206913808	0.272954479	0.96626	0.00008	0.00026	0.00004
-2	-0.5	0.004588325	0.004588325	0.96661	0.00000	0.00001	0.00000
-2	0.5	0.029763514	0.443217134	0.96819	0.00075	0.00023	0.00014
-2	1	0.156851516	0.949387718	0.96822	0.00068	0.00048	0.00027
-2	2	0.136564666	1.897559877	0.96821	0.00076	0.00101	0.00061
-2	3	0.136564666	3.081213589	0.96795	0.00074	0.00124	0.00094
-2	4	0.272954479	4.668452371	0.96831	0.00072	0.00240	0.00132
-2	5	0.443217134	6.158482111	0.96816	0.00065	0.00271	0.00162
-2	6	0.626603016	8.124084578	0.96845	0.00049	0.00437	0.00165
-2	7	0.826595874	10.717048299	0.96837	0.00055	0.00517	0.00237
-2	8	0.413562692	15.151342925	0.96839	0.00058	0.00663	0.00313
-2	9	1.438449888	21.420374904	0.96851	0.00042	0.00914	0.00373
-2	10	1.168608855	148.912903244	0.96870	0.00044	0.02394	0.01539
-2	11	0.771290612	138.949549437	0.96830	0.00100	0.02167	0.01493
-2	12	0.719685673	129.652816299	0.96815	0.00038	0.02310	0.01605
-2	13	0.826595874	120.978102069	0.96791	0.00038	0.02250	0.01662
-2	14	1.090420443	112.883789168	0.96781	0.00032	0.02469	0.01575
-2	15	0.626603016	105.331044537	0.96770	0.00032	0.02441	0.01416
-2	16	1.090420443	105.331044537	0.96750	0.00035	0.02457	0.01564
-3	-16	3.792690191	37.275937203	0.96775	0.00092	0.01680	0.00489
-3	-15	4.356099031	32.454744574	0.96787	0.00073	0.01604	0.00422
-3	-14	5.003202954	26.366508987	0.96811	0.00055	0.01483	0.00334
-3	-13	5.746434969	19.987196387	0.96838	0.00040	0.01342	0.00235
-3	-12	6.158482111	16.237767392	0.96865	0.00025	0.01237	0.00173
-3	-11	7.580524368	12.309079139	0.96890	0.00007	0.01143	0.00079
-4	-16	69.519279618	225.623046297	0.96855	0.00028	0.02101	0.00223
-4	-15	85.571831449	171.034100034	0.96884	0.00011	0.01972	0.00125

Table 3: Same as Table 1, but for Branch 3.

	n_s	r
branch1	0.96743 ± 0.00136	0.03819 ± 0.01298
branch2	0.96655 ± 0.00208	0.03193 ± 0.01605
branch3	0.96754 ± 0.00162	0.01492 ± 0.01386

Table 4: Summary of the predicted spectral index (n_s) and tensor-to-scalar ratio (r) for each branch, together with their uncertainties.

Branch: branch1

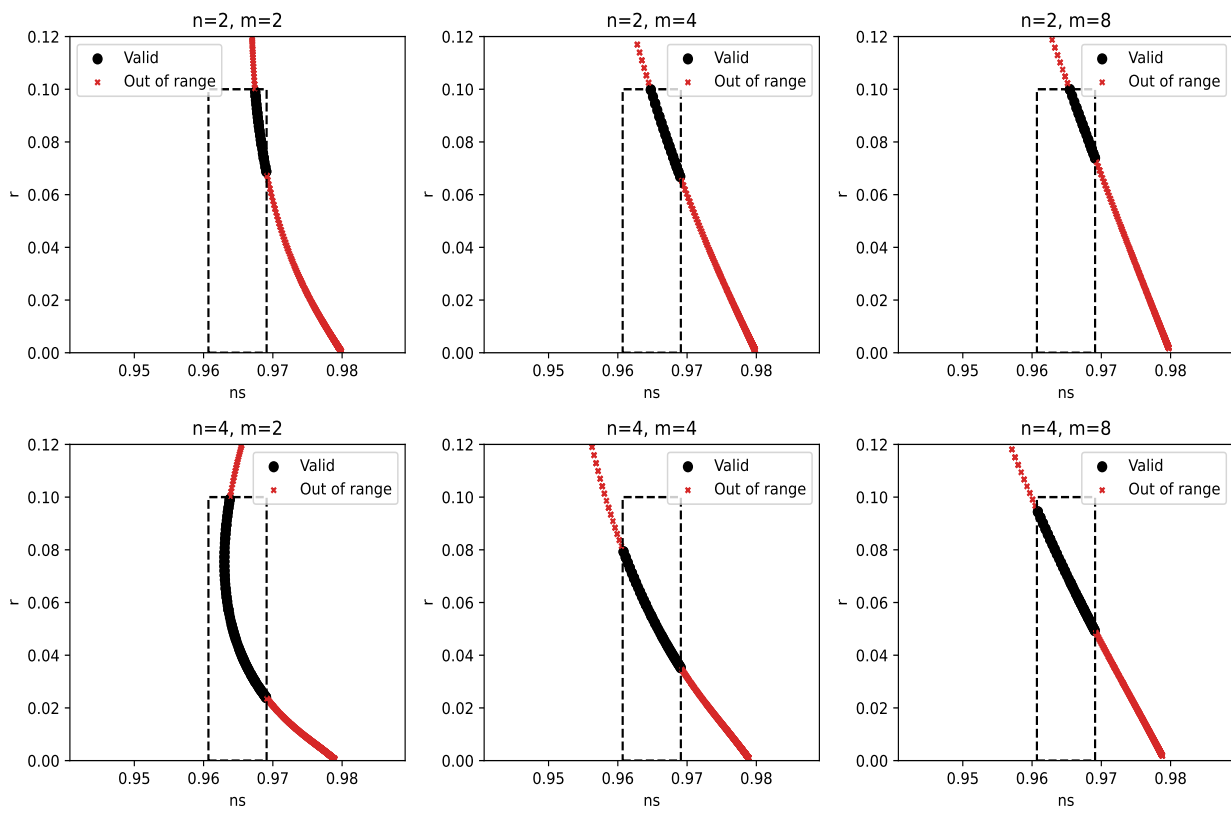


Figure 4.1: Parametric plots of the spectral index n_s and tensor-to-scalar ratio r for various (n, m) in Branch 1. The solid circles indicate parameter sets that satisfy observational constraints, while crosses correspond to values outside the allowed region.

Branch: branch2

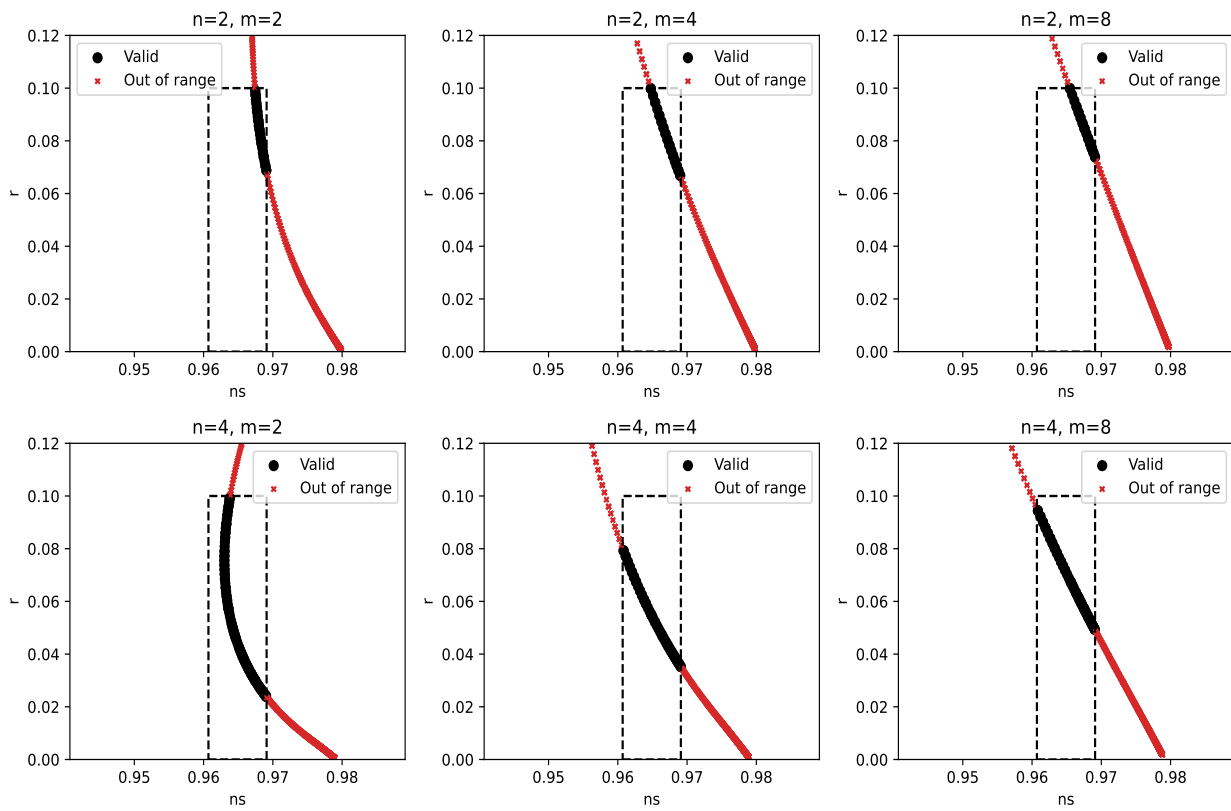


Figure 4.2: Same as Figure 4.1, but for Branch 2.

Branch: branch3

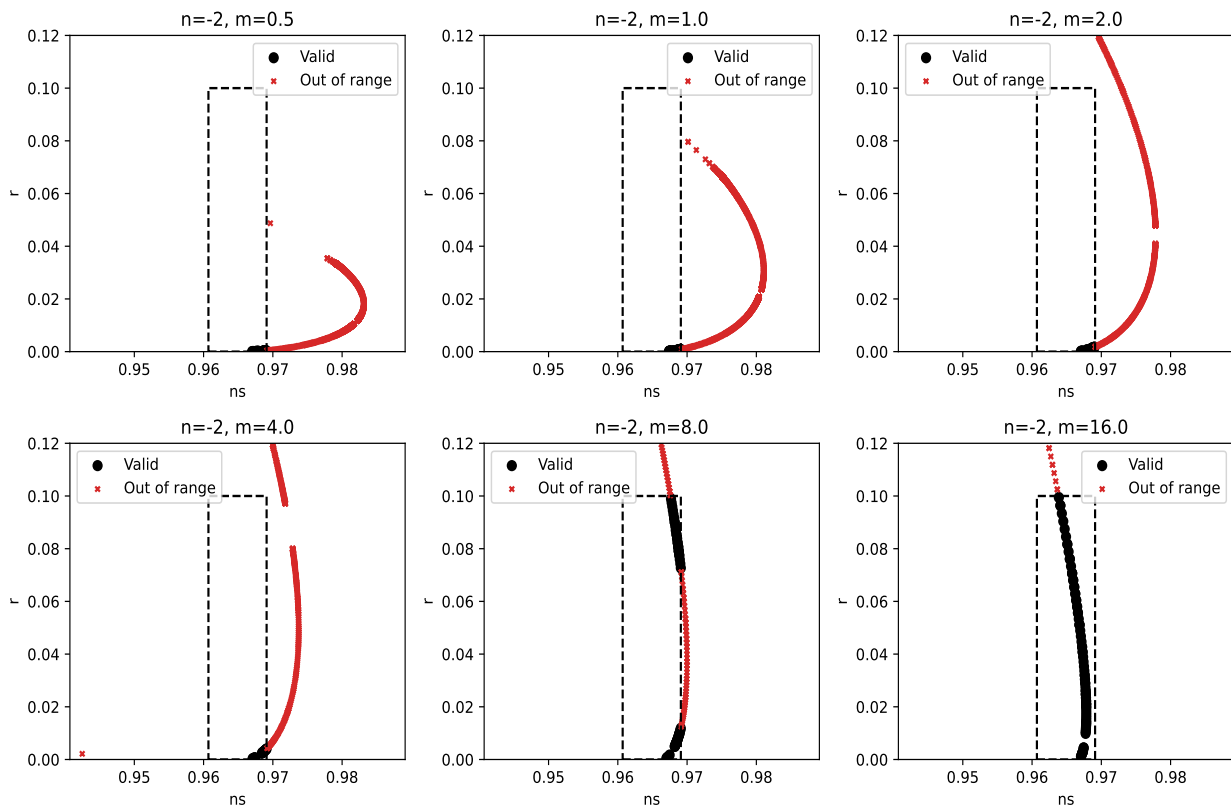


Figure 4.3: Same as Figure 4.1, but for Branch 3.

5 Overview of Approximate Analytical Results

In previous calculations, for the cases $n \neq -2$, the potential can be approximated as

$$V_\chi^{(m,n)}(\chi_n) \approx \frac{\lambda_m}{m} \left| \frac{A_n \chi_n^{\frac{1}{n+2}}}{\left(1 - n\theta(A_n)^n \chi_n^{\frac{n}{n+2}}\right)^{1/n}} \right|^m. \quad (5.1)$$

This approximation allows us to analyze, in a parametric way, how the predictions for n_s and r depend on the parameters n, m, θ and the e-folding number N_e .

The details of the derivation are provided in Appendix B¹⁵. Here, we summarize the main results. Using the standard slow-roll inflationary formalism, the spectral index n_s and the tensor-to-scalar ratio r can be approximated as

$$n_s = 1 - M_{pl}^2 \left(\frac{m}{n+2} \frac{1}{\chi_n} - \frac{m}{n} \delta_1 \right)^2 + 2M_{pl}^2 \left(-\frac{m}{n+2} \frac{1}{\chi_n} - \frac{m}{n} \delta_2 \right), \quad (5.2)$$

$$r = 8M_{pl}^2 \left(\frac{m}{n+2} \frac{1}{\chi_n} - \frac{m}{n} \delta_1 \right)^2. \quad (5.3)$$

Here, δ_1 and δ_2 collect the higher-order corrections arising from the derivatives of $V(\chi_n)$; see Appendix B for full details. Explicitly, they are given by

$$\delta_1 \equiv \frac{-n\theta A_n^n \frac{n}{n+2} \chi_n^{\frac{-2}{n+2}}}{1 - n\theta A_n^n \chi_n^{\frac{n}{n+2}}}, \quad (5.4)$$

$$\delta_2 \equiv \frac{-n\theta A_n^n \frac{-2n}{(n+2)^2} \chi_n^{\frac{-2}{n+2}-1}}{1 - n\theta A_n^n \chi_n^{\frac{n}{n+2}}} + \frac{-\frac{n^3}{(n+2)^2} \theta^2 A_n^{2n} \chi_n^{\frac{-4}{n+2}}}{\left(1 - n\theta A_n^n \chi_n^{\frac{n}{n+2}}\right)^2}. \quad (5.5)$$

The variable χ_n represents the value of the inflaton field at the beginning of inflation, which can be determined from the e-folding number N_e and the field value χ_{end} at the end of inflation (defined by $\epsilon_{end} = 1$). The behaviors of N, χ and χ_{end} differ for the case $-2 < n < 0$ compared to other ranges; see Appendix B for further discussion.

Our numerical analysis in the previous section revealed that solutions consistent with observations are found for positive n with negative θ , while for negative n with positive θ , no viable solutions within the observational bounds were obtained in the scanned range. This behavior can also be qualitatively understood from the approximate analytical calculation: the asymptotic structure of the potential and the dependence of n_s and r on (n, θ) follow similar trends.

Figure 5.1 displays the allowed region in the (n, θ) -plane where the predicted values of (n_s, r) satisfy $0.9067 < n_s < 0.9691$ and $r < 0.056$. The color scale indicates $\log_{10} r$, with smaller values of r shown in blue and larger values in red. It is apparent that solutions consistent with observations are only found for positive n with negative θ , while for negative n , no viable solutions exist within the scanned parameter range.

From the sign of n , one can see that the direction of squeezing (i.e., the action of the Virasoro generator L_n) must be reversed for negative n compared to positive n . As n increases, the squeezing effect becomes stronger, enabling the observational constraints to be satisfied even for smaller values of θ . However, excessive squeezing can cause the predictions to deviate from the observed values. Overall, for positive n , a broader range of θ satisfies the observational constraints, and the resulting scalar-to-tensor ratio r can be extremely small.

¹⁵Here, $M_{pl} \equiv 1/\sqrt{8\pi G}$ denotes the reduced Planck mass.

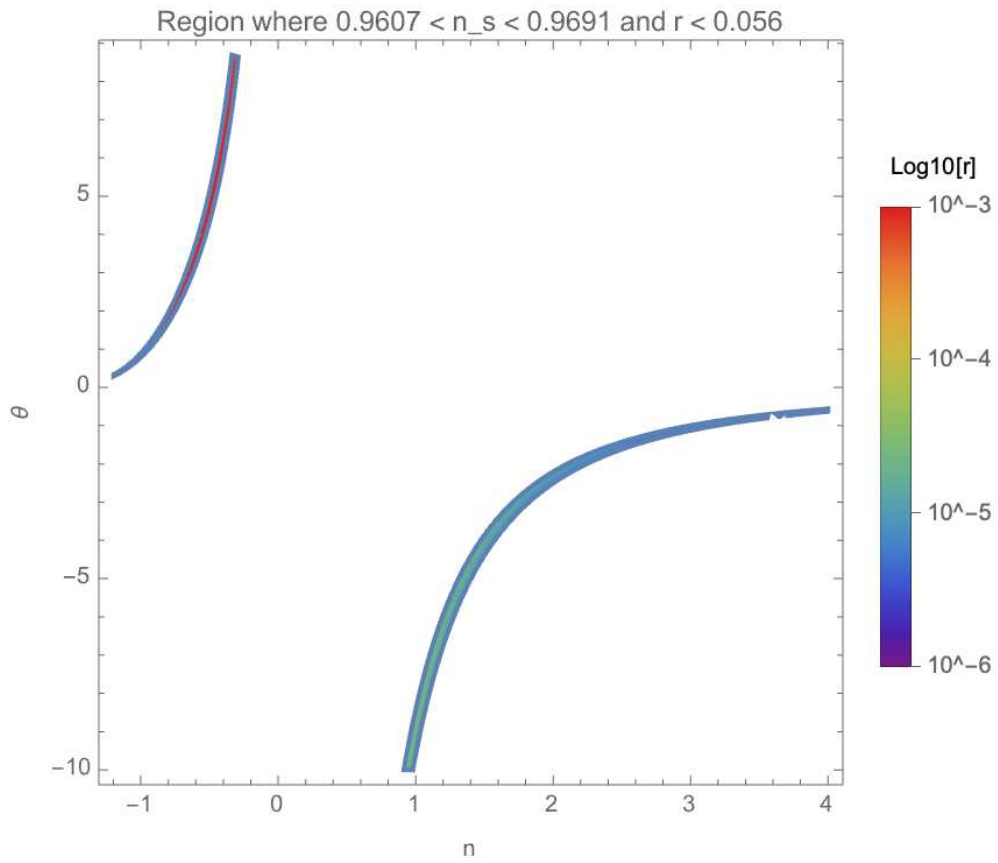


Figure 5.1: Allowed region in the (n, θ) parameter space where the predicted spectral index n_s and tensor-to-scalar ratio r satisfy the observational constraints $0.9607 < n_s < 0.9691$ and $r < 0.056$. The color scale represents $\log_{10} r$.

6 Conclusion and Discussion

In this paper, we have proposed a new class of inflationary models, termed “Virasoro inflation,” constructed by applying a conformal transformation to a complex scalar field. The transformation is generated by Virasoro generators L_n ($n = 0, \pm 1, \pm 2, \dots$) and parametrized by a continuous parameter θ . so that each model is specified by the pair (n, θ) .

A key assumption in our construction is that the conformal transformation is canonical, preserving the canonical conjugate relations. This naturally induces squeezing-like effects in the scalar field sector.

Under this framework, the original scalar potential $V(\phi^\dagger\phi) = \frac{\lambda m}{m} |\phi(t)|^m$ is mapped into a new potential $V_\chi^{(m)}(\chi_n)$ for a redefined field $\chi_n(t)$, which ensures the kinetic term remains canonical. The modulus of the new field, $|\chi_n(t)|$ plays the role of the inflaton, slowly rolling down the transformed potential $V_\chi^{(m)}(\chi_n)$.

This construction yields a wide variety of novel inflationary models. Among them, models with positive n are shown to produce predictions for the spectral index n_s and tensor-to-scalar ratio r that are consistent with current CMB observations, under suitable choices of (m, θ) and for typical e-folding numbers ($N_e = 50-60$). In this paper, we have presented detailed results for $N_e = 60$ as a representative case.

A notable advantage of our framework is its simplicity: the transformation acts solely on the scalar field, without any need for conformal coupling to gravity. Moreover, the plateau structure of the transformed potential emerges generically from the maximum modulus theorem in complex analysis. Under a holomorphic and singularity-free transformation

$$\phi \rightarrow \chi = F(\phi), \tag{6.1}$$

the potential

$$V_\chi(\chi) = |W(\chi)|^2 = V_\phi(F(\phi)^\dagger F(\phi)) \tag{6.2}$$

attains its maximum only on the boundary $|\chi| \rightarrow \infty$. Therefore, the interior of the field space exhibits a natural plateau.

We have also assumed that the squeezing effect occurs just before the onset of inflation. As a possible physical origin, we briefly discussed analogies with higher-order squeezing mechanisms in quantum optics.

It is intriguing to speculate whether the conformal squeezing studied here might be related to effective dynamics in brane systems, such as M2–M5 configurations, where Virasoro-like symmetries and holomorphic deformations naturally emerge. One possible manifestation of such effective dynamics is the appearance of friction-like terms in the inflaton’s evolution. These terms do not correspond to conventional dissipation, but may instead encode geometric resistance arising from spontaneous symmetry breaking or nontrivial twisting between intersecting branes, leading to effective non-conservative behavior at low energies.

We leave a detailed investigation of these possible connections, as well as further phenomenological implications of Virasoro inflation, as interesting directions for future research.

Acknowledgments

The authors would like to thank Shiro Komata for carefully reading the manuscript and providing valuable comments. They are also grateful to the members of the theoretical seminar group at the Open University of Japan for their helpful feedback and for providing a stimulating environment in which to share ongoing progress.

A Numerical Setup Detail

A.1 Numerical Procedure

To evaluate the inflationary observables n_s and r for a given Virasoro inflation model, we follow a numerical procedure that avoids the analytical approximations used in Section 4. The key idea is to solve the end-of-inflation condition and the e-folding number integral numerically, based on the transformed potential.

The overall algorithm proceeds as follows:

Algorithm: Numerical Procedure for Computing n_s and r

- 1: **Input:** Virasoro index n , potential power m , dimensionless parameter $\bar{\theta}$, e-folding number N_e
- 2: Select branch depending on sign of n :
- 3: **if** $n > 0$ **then**
- 4: Use Branch 2+
- 5: **else**
- 6: Use Branch 3–
- 7: **end if**
- 8: Define dimensionless variables $y = \bar{F}_n(\phi)$, $x = \bar{\chi}_n$
- 9: Obtain analytical forms of $y(x)$, $y'(x)$, and $y''(x)$ from Appendix B
- 10: Solve for y_e satisfying:

$$\epsilon_V(y_e) = \frac{1}{2}m^2|n|^{2/n}|\bar{\theta}|^{2/n} \left(\frac{y'}{y}\right)^2 = 1$$

- 11: Solve for y_b using the e-folding condition:

$$N_e = \frac{1}{m|n\bar{\theta}|^{2/n}} \int_{y_e}^{y_b} \frac{y}{(y')^2} dy$$

- 12: Compute slow-roll parameters at $y = y_b$:

$$\epsilon_V = \frac{1}{2}m^2|n|^{2/n}|\bar{\theta}|^{2/n} \left(\frac{y'}{y}\right)^2$$

$$\eta_V = |n|^{2/n}|\bar{\theta}|^{2/n} \left[m(m-1) \left(\frac{y'}{y}\right)^2 + m\frac{y''}{y} \right]$$

- 13: Evaluate observables:

$$n_s = 1 - 6\epsilon_V + 2\eta_V, \quad r = 16\epsilon_V$$

- 14: **Output:** n_s, r
-

This procedure enables us to explore the full parameter space $(n, m, \bar{\theta})$, including the subtleties arising from branch selection in the Virasoro transformation. Analytical forms for y , y' and y'' specific to each branch are listed in next Section.

A.2 List of y

The conformal transformation $\phi \rightarrow F_n(\phi; \theta)$ is generated by the n -th Virasoro generator with a complex parameter θ , and is given by

$$F_n(\phi; \theta) = \phi_n(\theta) = \frac{\phi}{(1 - n\theta\phi^n)^{1/n}}. \quad (\text{A.1})$$

This conformal transformation maps the original complex scalar field model defined by ϕ into a new scalar field model characterized by χ_n , which plays the role of the inflaton field in the transformed theory.

The relation between ϕ and χ is given by

$$\chi_n(\phi) = \int_0^\phi \frac{d\phi}{F'_n(\phi)} = \int_0^\phi d\phi (1 - n\theta\phi^n)^{1+1/n} = \int_0^\phi d\phi \frac{\phi^{n+1}}{F_n(\phi)^{n+1}}. \quad (\text{A.2})$$

The potential V_χ is derived from the original potential $V_\phi = \frac{\lambda}{m}|\phi|^m$ as

$$V_\chi = \frac{\lambda}{m}|F_n(\phi)|^m. \quad (\text{A.3})$$

All fields are assumed to have the same mass dimension $[M]$, while the potential has mass dimension $[M^4]$. The mass dimension of the scalar field in four-dimensional spacetime is $[\phi] = [M]$. From the form of the conformal transformation, the mass dimension of θ is given by

$$[\theta] = [M^{-n}]. \quad (\text{A.4})$$

The field χ has the same dimension as ϕ , namely $[\chi] = [M]$.

We now define the corresponding dimensionless quantities $\bar{\phi}$, $\bar{\chi}_n$, \bar{F}_n and \bar{V}_χ by absorbing the common factor $n\theta$ as follows:

$$|n\theta|\phi^n = \bar{\phi}^n, \text{ or equivalently } \phi = \frac{\bar{\phi}}{|n\theta|^{1/n}}, \quad (\text{A.5})$$

$$\chi = \frac{\bar{\chi}}{|n\theta|^{1/n}}, \quad F_n = \frac{\bar{F}_n}{|n\theta|^{1/n}}, \quad V_\chi = \frac{\bar{V}_\chi}{|n\theta|^{4/n}}. \quad (\text{A.6})$$

Here, we introduce a dimensionless squeezing parameter $\bar{\theta} = \theta M_{pl}^n$. Thus, the model is fully specified by the set of parameters $(n, m, \bar{\theta})$. We express all relevant equations in terms of two dimensionless variables, $\bar{F}_n = y$ and $\bar{\chi}_n = x$, so that the formulation can be consistently described using the pair (x, y) . When performing the integration, we change the integration variable from ϕ to a new variable t .

The transformation rule for the integration variable is given as follows:

- For $n > 0$: Since ϕ increases monotonically,

$$t = |n\theta|\phi^n \equiv \bar{\phi}^n. \quad (\text{A.7})$$

- For $n < 0$: As ϕ becomes large, $\phi^{|n|}$ becomes small, and therefore

$$\frac{1}{t} = |n\theta|\phi^{-|n|} \text{ or } t = \frac{\phi^{|n|}}{|n\theta|} = \bar{\phi}^{|n|}. \quad (\text{A.8})$$

The conformal transformation

$$F_n(\phi; \theta) = \phi_n(\theta) = \frac{\phi}{(1 - n\theta\phi^n)^{1/n}} \quad (\text{A.9})$$

can be rewritten using the rescaled variables introduced earlier. Specifically, we define

$$y = \bar{F}_n = |n\theta|^{1/n} F_n(\phi; \theta) = |n\theta|^{1/n} \phi_n(\theta) = \frac{\bar{\phi}}{(1 - \text{sgn}(n\theta)\bar{\phi}^n)^{1/n}}. \quad (\text{A.10})$$

Here, we introduce $\epsilon = \text{sgn}(\theta)$.

Thus, we have

$$y = \frac{\bar{\phi}}{(1 - \text{sgn}(n\theta)\bar{\phi}^n)^{1/n}}. \quad (\text{A.11})$$

We now re-express this equation in terms of the variable t .

At this point, the sign of n introduces branching behavior, since the denominator involves an n -th root, which requires careful branch selection. The choice of branch determines whether the transformed potential exhibits a plateau structure, which is essential for satisfying the slow-roll conditions.

- For $n > 0$ (denoted as Branch2+), we use $t = |n\theta|\phi^n \equiv \bar{\phi}^n$. Since $\text{sgn}(n\theta) = \epsilon$, we have

$$y = \frac{t^{1/n}}{(1 - \epsilon t)^{1/n}} = t^{1/n} (1 - \epsilon t)^{1/n}. \quad (\text{A.12})$$

- For $n < 0$ (denoted as Branch3-), we use $t = \bar{\phi}^{|n|}$, and since $\text{sgn}(n\theta) = -\epsilon$, we obtain

$$y = \frac{t^{1/|n|}}{(1 + \epsilon t^{-1})^{-1/|n|}} = \left(\frac{t^{-1}}{(1 + \epsilon t^{-1})} \right)^{-1/|n|} = (t + \epsilon)^{1/|n|}. \quad (\text{A.13})$$

- [Branch1+] uses the same substitution as Branch 2+, namely $t = |n\theta|\phi^n$. However, it differs in the way the n -th root in the denominator is taken. We start by using the identity

$$y = \frac{t^{1/n}}{(1 - \epsilon t)^{1/n}}, \quad (\text{A.14})$$

which corresponds to the principal branch used in Branch 2+. Here, we consider an alternative way of taking the n -th root. By rewriting the denominator, we obtain

$$(1 - \epsilon t)^{1/n} = \left(-\epsilon\left(-\frac{1}{\epsilon} + t\right)\right)^{1/n} = (-\epsilon)^{1/n}(t - \epsilon)^{1/n}, \quad (\text{A.15})$$

where we have used the identity $(-\epsilon)\epsilon = -1$. With this substitution, the expression for y becomes

$$y = \frac{t^{1/n}}{(-\epsilon)^{1/n}(t - \epsilon)^{1/n}}. \quad (\text{A.16})$$

This is still consistent with the form of Branch 2+, but in Branch 1+, we take a different branch of the n -th root such that the prefactor $(-\epsilon)^{-1/n}$ is eliminated. This leads to the final expression

$$y = \frac{t^{1/n}}{(t - \epsilon)^{1/n}}. \quad (\text{A.17})$$

To summarize, the three branches are defined as follows:

- [Branch1+] (for $n > 0$)

$$\begin{aligned} \text{Variable substitution : } t &= |n\theta|\phi^n \equiv \bar{\phi}^n \\ \text{Resulting expression : } y &= \frac{t^{1/n}}{(t - \epsilon)^{1/n}} \end{aligned} \quad (\text{A.18})$$

- [Branch2+] (for $n > 0$)

$$\begin{aligned} \text{Variable substitution : } t &= |n\theta|\phi^n \equiv \bar{\phi}^n \\ \text{Resulting expression : } y &= t^{1/n}(1 - \epsilon t)^{-1/n} \end{aligned} \quad (\text{A.19})$$

- [Branch3-] (for $n < 0$)

$$\begin{aligned} \text{Variable substitution : } t &= \frac{\phi^{|n|}}{|n\theta|} = \bar{\phi}^{|n|} \\ \text{Resulting expression : } y &= (t + \epsilon)^{1/|n|} \end{aligned} \quad (\text{A.20})$$

B Summary of Perturbative Calculations

This appendix summarizes the details of the perturbative calculations in the Virasoro-squeezing inflationary model.

B.1 Classification of Potential Structures and Variable Transformations by n

We consider a class of inflationary models in which a scalar field ϕ is subject to a Virasoro squeezing transformation defined by

$$F_n(\phi) = \left(\frac{1}{1 - n\theta\phi^n} \right)^{\frac{1}{n}} \phi. \quad (\text{B.1})$$

Here, the parameter n specifies which Virasoro generator L_n is used in the squeezing, and θ controls the strength of the squeezing. The potential is then given by

$$V_m = \frac{1}{m} \lambda_m |F_n(\phi)|^m. \quad (\text{B.2})$$

In accordance with this transformation, we introduce a new scalar field χ_n that preserves the canonical kinetic term. It is defined through the differential relation:

$$\frac{d\chi_n}{d\phi} = \frac{1}{F'(\phi)} \Rightarrow \chi_n = \int^\phi \frac{1}{F'_n(\phi)} d\phi = \int^\phi (1 - n\theta\phi^n)^{1+\frac{1}{n}} d\phi. \quad (\text{B.3})$$

This variable transformation rewrites the potential as a function of χ_n , which will henceforth serve as the inflaton field in the analysis.

The behavior of this integral varies depending on the sign and magnitude of the exponent n , leading to qualitatively different approximations in different regimes. In the remainder of this section, we classify the potential structures according to the domain of n , and derive approximate expressions accordingly.

B.1.1 Case $n > 0$: Dominance in the Large- ϕ Regime

In this case, the integral is dominated by the region where $\phi \rightarrow \infty$. Therefore, we have

$$\chi_n \approx \int^\phi (-n\theta\phi^n)^{1+\frac{1}{n}} d\phi \propto \phi^{n+2} \quad (\text{B.4})$$

which implies the inverse relation

$$\phi(\chi_n) \approx A_n \chi_n^{\frac{1}{n+2}}, \quad A_n = \left(\frac{n+2}{(-n\theta)^{1+\frac{1}{n}}} \right)^{\frac{1}{n+2}}. \quad (\text{B.5})$$

Accordingly, the potential can be approximated as

$$V_m \approx \frac{\lambda_m}{m} \left| \frac{A_n \chi_n^{\frac{1}{n+2}}}{\left(1 - n\theta A_n^n \chi_n^{\frac{n}{n+2}}\right)^{\frac{1}{n}}} \right|^m. \quad (\text{B.6})$$

In the limit $\chi_n \rightarrow \infty$, this potential asymptotically approaches a plateau, thereby naturally satisfying the slow-roll conditions required for inflation.

B.1.2 Case $n < -2$: Dominance in the Small- ϕ Regime

When $n < 0$, the integral is dominated by the region near $\phi \rightarrow 0$. In particular, for $n < -2$, we find

$$\chi_n(\phi) \approx \int^\phi \left(|n|\theta\phi^{-|n|} \right)^{1-\frac{1}{|n|}} d\phi \propto \phi^{2-|n|}, \quad (\text{B.7})$$

which implies the inverse relation

$$\phi(\chi_n) \approx B_n \chi_n^{\frac{1}{2-|n|}}, \quad B_n = \left(\frac{-|n|+2}{(|n|\theta)^{1-\frac{1}{|n|}}} \right)^{\frac{1}{2-|n|}}. \quad (\text{B.8})$$

In this case as well, the potential exhibits a plateau as $\chi_n \rightarrow \infty$. Formally, the structure is nearly identical to the case $n > 0$ discussed in the previous subsection, and the derivation of inflationary observables proceeds in a parallel manner.

B.1.3 Case $-2 < n < 0$: Necessity of Corrections in the Intermediate Regime

In this case, since the exponent $\frac{1}{2-|n|} > 1$, the approximate expansion $\phi(\chi_n)$ remains valid. However, higher-order corrections cannot be neglected when deriving the slow-roll parameters.

Indeed, for the integral expression of the e-folding number,

$$N_e \simeq \frac{1}{M_{pl}^2} \int_{\chi_{end}}^{\chi} \left(\frac{d \log V}{d \chi_n} \right)^{-1} d \chi_n, \quad (\text{B.9})$$

a simple power-law approximation is insufficient. It becomes necessary to incorporate correction terms such as $\chi_n^{n/(n+2)}$, as well as perturbative terms like δ (discussed later).

Physically, this parameter range is also special, since the plateau of the potential does not necessarily appear in the limit $\chi_n \rightarrow \infty$. As a result, the slow-roll condition is not automatically satisfied and must be treated with particular care.

B.2 Observable Quantities and Slow-Roll Parameters

The key cosmological observables, namely the spectral index n_s and the tensor-to-scalar ratio r , are given under the slow-roll approximation by the following expressions:

$$n_s - 1 \approx -6\epsilon_V + 2\eta_V, \quad (\text{B.10})$$

$$r \approx 16\epsilon_V. \quad (\text{B.11})$$

Here, ϵ_V and η_V are the slow-roll parameters, defined with respect to the potential $V(\chi_n)$ as

$$\epsilon_V \equiv \frac{M_{pl}^2}{2} \left(\frac{V_{,\chi}}{V} \right)^2 = \frac{M_{pl}^2}{2} \left(\frac{\partial}{\partial \chi} \log V \right)^2, \quad (\text{B.12})$$

$$\eta_V \equiv M_{pl}^2 \frac{V_{,\chi\chi}}{V}. \quad (\text{B.13})$$

The e-folding number N_e , which quantifies the amount of inflation, is defined with respect to the evolution of the inflaton field χ_n by the integral

$$N_e \simeq \frac{1}{M_{pl}^2} \int_{\chi_{end}}^{\chi} \left(\frac{d \log V}{d \chi_n} \right)^{-1} d \chi_n, \quad (\text{B.14})$$

where M_{pl} is the reduced Planck mass. The value of the field at the end of inflation, χ_{end} , is determined by the condition

$$\epsilon_V(\chi_{end}) \approx 1. \quad (\text{B.15})$$

Using these relations, the next subsection will carry out explicit calculations of ϵ_V and η_V , and derive theoretical predictions for the observables n_s and r .

B.3 Derivation of Slow-Roll Parameters and Analysis of Approximate Structures

In this subsection, we explicitly derive the slow-roll parameters ϵ_V and η_V for the inflaton potential. We begin by employing a simple power-law approximation for $\phi(\chi_n)$ in order to compute the slow-roll parameters.

As discussed in Section A.1, this approximation is valid for $n > 0$, or formally applicable to the entire range $n < 0$ as well. However, in the intermediate regime $-2 < n < 0$, it becomes necessary to incorporate correction terms, as will be discussed later.

B.3.1 Evaluation of ϵ_V

Based on the power-law approximation $\phi(\chi_n) \approx A_n \chi_n^{1/(n+2)}$, the potential can be written as

$$V_m \approx \frac{\lambda_m}{m} \left| \frac{A_n \chi_n^{\frac{1}{n+2}}}{\left(1 - n\theta A_n^n \chi_n^{\frac{n}{n+2}}\right)^{\frac{1}{n}}} \right|^m. \quad (\text{B.16})$$

Taking the logarithm, we can expand $\log V_m$ as

$$\log V_m = \log \lambda_m - \log m + m \log |A_n| + \frac{m}{n+2} \log |\chi_n| - \frac{m}{n} \log |1 - n\theta A_n^n \chi_n^{\frac{n}{n+2}}|. \quad (\text{B.17})$$

By differentiating this expression, the slow-roll parameter ϵ_V is given by

$$\epsilon_V = \frac{M_{pl}^2}{2} \left(\frac{\partial}{\partial \chi} \log V \right)^2. \quad (\text{B.18})$$

Explicitly differentiating $\log V_m$, we obtain

$$\frac{d \log V_m}{d \chi_n} = \frac{m}{n+2} \frac{1}{\chi_n} - \frac{m}{n} \left(\frac{-n\theta A_n^n \frac{n}{n+2} \chi_n^{\frac{-2}{n+2}}}{1 - n\theta A_n^n \chi_n^{\frac{n}{n+2}}} \right). \quad (\text{B.19})$$

Therefore, the slow-roll parameter ϵ_V becomes

$$\epsilon_V = \frac{M_{pl}^2}{2} \left(\frac{m}{n+2} \frac{1}{\chi_n} - \frac{m}{n} \left(\frac{-n\theta A_n^n \frac{n}{n+2} \chi_n^{\frac{-2}{n+2}}}{1 - n\theta A_n^n \chi_n^{\frac{n}{n+2}}} \right) \right)^2. \quad (\text{B.20})$$

This expression becomes particularly useful in the large- χ_n limit (i.e., during the early stage of inflation), where the dominant terms are clearly identified and can be used for further simplification.

B.3.2 Evaluation of η_V

The slow-roll parameter η_V involves the second derivative of the potential and is defined by

$$\begin{aligned} \eta_V = M_{pl}^2 & \left(-\frac{m}{n+2} \frac{1}{\chi_n^2} \right. \\ & - \frac{m}{n} \left(\frac{-n\theta A_n^n \frac{-2n}{(n+2)^2} \chi_n^{\frac{-2}{n+2}-1}}{1 - n\theta A_n^n \chi_n^{\frac{n}{n+2}}} + \frac{-\frac{n^3}{(n+2)^2} \theta^2 A_n^{2n} \chi_n^{\frac{-4}{n+2}}}{\left(1 - n\theta A_n^n \chi_n^{\frac{n}{n+2}}\right)^2} \right) \\ & \left. + \left(\frac{m}{n+2} \frac{1}{\chi_n} - \frac{m}{n} \left(\frac{-n\theta A_n^n \frac{n}{n+2} \chi_n^{\frac{-2}{n+2}}}{1 - n\theta A_n^n \chi_n^{\frac{n}{n+2}}} \right) \right)^2 \right). \end{aligned} \quad (\text{B.21})$$

This expression, together with that of ϵ_V , will be used in the subsequent evaluation of the inflationary observables n_s and r .

B.3.3 Connection to Observables

Using the slow-roll parameters ϵ_V and η_V , the inflationary observables—namely, the spectral index n_s and the tensor-to-scalar ratio r —are given by

$$n_s - 1 \approx -6\epsilon_V + 2\eta_V, \quad (\text{B.22})$$

$$r \approx 16\epsilon_V. \quad (\text{B.23})$$

By substituting the expressions for ϵ_V and η_V derived in the previous subsections, these equations provide theoretical predictions for n_s and r as functions of the inflaton field χ_n .

In the next subsection, we use these results to evaluate the relationship between χ_n and the e-folding number, and to obtain concrete predictions.

B.4 Evaluation of the E-Folding Number and the Field Values χ , χ_{end}

During inflation, the e-folding number N_e is given under the slow-roll approximation by

$$N_e \simeq \frac{1}{M_{pl}^2} \int_{\chi_{end}}^{\chi} \left(\frac{d \log V}{d\chi_n} \right)^{-1} d\chi_n. \quad (\text{B.24})$$

Here, the field value χ_{end} at the end of inflation is determined by the condition that the slow-roll parameter ϵ_V reaches unity:

$$\epsilon_V(\chi_{end}) \approx 1. \quad (\text{B.25})$$

Using the approximate expression of $\epsilon_V(\chi_n)$ derived earlier, this condition can be treated as an equation for χ_{end} , which can then be solved approximately.

Throughout the following discussion, we introduce the notation $(\pm)_{(0)}$ to explicitly indicate the sign of χ_{end} . Although the actual sign may vary depending on the context, we adopt this notation for notational consistency, under the assumption that the physical field magnitude is treated as positive.

B.4.1 Case $n > 0$ and $n < -2$

In this case, the field value χ_n is sufficiently large, and the condition $n\theta A_n^n \chi_n^{n/(n+2)} \ll 1$ holds. Under this assumption, the following approximation is valid:

$$\frac{d \log V_m}{d\chi_n} \approx \frac{m}{n+2} \frac{1}{\chi_n} - \frac{m}{n} \left(\frac{-n\theta A_n^n \frac{n}{n+2} \chi_n^{\frac{-2}{n+2}}}{1 - n\theta A_n^n \chi_n^{\frac{n}{n+2}}} \right). \quad (\text{B.26})$$

The e-folding number can then be evaluated as

$$N_e \simeq \frac{1}{M_{pl}^2} \int_{\chi}^{\chi_{end}} \left(\frac{m}{n+2} \frac{1}{\chi_n} - \frac{m}{n} \left(\frac{-n\theta A_n^n \frac{n}{n+2} \chi_n^{\frac{-2}{n+2}}}{1 - n\theta A_n^n \chi_n^{\frac{n}{n+2}}} \right) \right)^{-1} d\chi_n. \quad (\text{B.27})$$

This integral can be approximated in the limit $\chi_n \rightarrow \infty$, and it reduces to a power-law integral based on the variable transformation $\phi \sim \chi_n^{1/(n+2)}$. As a result of this approximation, we obtain the following relation:

$$N_e \simeq \frac{1}{M_{pl}^2} \frac{2n(n+1)}{m} \theta A_n^n \left(\chi_{end}^{\frac{n}{n+2}} - \chi^{\frac{n}{n+2}} \right). \quad (\text{B.28})$$

This expression represents the difference between χ_{end} and χ with an exponent depending on n , and can be used to determine the inflaton field value at the beginning of inflation.

Furthermore, from the condition $\epsilon_V(\chi_{end}) \approx 1$, we obtain the following approximate equation:

$$\frac{m}{n+2} \frac{1}{\chi_{end}} - \frac{m}{n} \left(\frac{-n\theta A_n^n \frac{n}{n+2} \chi_{end}^{\frac{-2}{n+2}}}{1 - n\theta A_n^n \chi_{end}^{\frac{n}{n+2}}} \right) \approx (\pm)_{(0)} \frac{\sqrt{2}}{M_{pl}}. \quad (\text{B.29})$$

Assuming that χ_{end} is sufficiently large such that $n\theta A_n^n \chi_{end}^{n/(n+2)} \ll 1$, we can expand the denominator to leading order and approximate:

$$-\frac{m}{n+2} \frac{1}{n\theta} A_n^{-n} \chi_{end}^{-1} \approx (\pm)_{(0)} \frac{\sqrt{2}}{M_{pl}}. \quad (\text{B.30})$$

Solving for χ_{end} , we obtain:

$$\chi_{end} \approx -(\pm)_{(0)} \frac{n(n+2)}{m} \frac{M_{pl}}{\sqrt{2}} n\theta A_n^{-n}. \quad (\text{B.31})$$

Substituting the above expression for χ_{end} into the previously derived formula for the e-folding number, we obtain the following expression for χ :

$$\chi = \chi_{end} \left(1 - \frac{2n(n+1)}{mN_e M_{pl}^2} \theta A_n^n \chi_{end}^{\frac{n}{n+2}} \right). \quad (\text{B.32})$$

This leads to a structure with a power-law correction:

$$\chi = -(\pm)_{(0)} \frac{n(n+2)}{m} \frac{M_{pl}}{\sqrt{2}} n\theta A_n^{-n} \left(1 - \frac{2n(n+1)}{mN_e M_{pl}^2} \theta A_n^n \left(-(\pm)_{(0)} \frac{n(n+2)}{m} \frac{M_{pl}}{\sqrt{2}} n\theta A_n^{-n} \right)^{\frac{n}{n+2}} \right). \quad (\text{B.33})$$

This expression serves as a fundamental formula for estimating the value of the inflaton field χ at the beginning of inflation in terms of the e-folding number N_e .

B.4.2 Case $-2 < n < 0$

In this case, the field value χ_n is not necessarily large, and the quantity $n\theta A_n^n \chi_n^{n/(n+2)}$ is not guaranteed to be small. As a result, the approximations used in the previous subsection—where leading-order terms cancel and correction terms dominate—are no longer applicable, and a different treatment is required.

Under this condition, the e-folding number can be approximated as

$$N_e \simeq \frac{1}{M_{pl}^2} \frac{m}{n+2} \left(\frac{1}{2} \chi_{end}^2 - \frac{1}{2} \chi^2 - n \left(\frac{n}{n+2} + 1 \right) \theta A_n^n \left(\chi_{end}^{\frac{n}{n+2}+2} - \chi^{\frac{n}{n+2}+2} \right) \right). \quad (\text{B.34})$$

This expression arises from an approximate integration with respect to χ_n , in which the leading-order power-law term χ^2 and the correction term $\chi^{n/(n+2)}$ are treated separately.

By inverting the above expression, we obtain an approximate expansion of χ as a function of the e-folding number N_e :

$$\chi \approx \chi_{end} \left(1 - \frac{2(n+2)}{m} N_e M_{pl}^2 \chi_{end}^{-2} - 2n \frac{2n+2}{n+2} \theta A_n^n \chi_{end}^{\frac{n}{n+2}} \left(\chi_{end}^{\frac{n}{n+2}} - \chi^{\frac{n}{n+2}} \right) \right)^{\frac{1}{2}}. \quad (\text{B.35})$$

Expanding the power and reorganizing the terms perturbatively, we arrive at a simpler form:

$$\chi \approx \chi_{end} \left(1 - \frac{(n+2)}{m} N_e M_{pl}^2 \chi_{end}^{-2} - n \frac{2n+2}{n+2} \theta A_n^n \chi_{end}^{\frac{n}{n+2}} \left(\chi_{end}^{\frac{n}{n+2}} - \chi^{\frac{n}{n+2}} \right) \right). \quad (\text{B.36})$$

Moreover, the value of χ_{end} is approximately determined by the condition $\epsilon_V(\chi_{end}) \approx 1$, leading to

$$\chi_{end} \approx (\pm)_0 \frac{n+2}{m} \frac{M_{pl}}{\sqrt{2}} \left(1 + ((\pm)_0)^{\frac{n}{n+2}} n\theta A_n^n \left(\frac{n+2}{m} \frac{M_{pl}}{\sqrt{2}} \right)^{\frac{n}{n+2}} \right). \quad (\text{B.37})$$

Accordingly, χ can also be expanded in the same manner as

$$\chi \approx (\pm)_0 \frac{n+2}{m} \frac{M_{pl}}{\sqrt{2}} \left(1 + ((\pm)_0)^{\frac{n}{n+2}} n\theta A_n^n \left(\frac{n+2}{m} \frac{M_{pl}}{\sqrt{2}} \right)^{\frac{n}{n+2}} \right) \left(1 - 2 \frac{mN_e}{n+2} \right). \quad (\text{B.38})$$

In this way, for the case $-2 < n < 0$, it is necessary to explicitly retain both the power-law correction and the perturbative contributions. This requires a different treatment from that in the previous subsection.

B.5 Crude Estimation

In this subsection, we use the approximate expressions for χ and χ_{end} derived in the previous subsection, along with the leading-order contributions of the slow-roll parameters, to obtain a crude estimate of the inflationary observables n_s and r .

These observables are given in terms of the slow-roll parameters ϵ_V and η_V as follows:

$$n_s \approx 1 - 6\epsilon_V + 2\eta_V, \quad r \approx 16\epsilon_V. \quad (\text{B.39})$$

Under the power-law approximation, we may assume that χ is sufficiently large, which allows the following leading-order approximations for the slow-roll parameters:

$$\epsilon_V \approx \frac{M_{pl}^2}{2} \left(\frac{m}{n+2} \frac{1}{\chi} - \frac{m}{n} \left(\frac{-\frac{n}{n+2}\chi^{-1}}{n^{-1}\theta^{-1}A_n^{-n}\chi^{-\frac{n}{n+2}} - 1} \right) \right)^2, \quad (\text{B.40})$$

$$\begin{aligned} \eta_V \approx & M_{pl}^2 \left(-\frac{m}{n+2} \frac{1}{\chi^2} \right. \\ & - \frac{m}{n} \left(\frac{-n\theta A_n^n \frac{-2n}{(n+2)^2} \chi^{\frac{-2}{n+2}-1}}{1 - n\theta A_n^n \chi^{\frac{n}{n+2}}} + \frac{-\frac{n^3}{(n+2)^2} \theta^2 A_n^{2n} \chi^{\frac{-4}{n+2}}}{(1 - n\theta A_n^n \chi^{\frac{n}{n+2}})^2} \right) \\ & \left. + \left(\frac{m}{n+2} \frac{1}{\chi} - \frac{m}{n} \left(\frac{-n\theta A_n^n \frac{-n}{n+2} \chi^{\frac{-2}{n+2}}}{1 - n\theta A_n^n \chi^{\frac{n}{n+2}}} \right) \right)^2 \right). \end{aligned} \quad (\text{B.41})$$

The field value χ in these expressions can be substituted using the approximate solution obtained in the previous subsection. The observables n_s and r can then be evaluated either numerically or through these analytical approximations.

B.6 Estimation of Errors

We now estimate the accuracy of the approximation

$$\phi(\chi_n) \approx A_n \chi_n^{1/(n+2)} \quad (\text{B.42})$$

which has been used throughout the previous analysis. To do so, we consider a perturbed form with a correction term δ :

$$\phi(\chi_n) \approx (A_n \chi_n^{\frac{1}{n+2}}) (1 + \delta), \quad (\text{B.43})$$

and evaluate perturbatively how accurate this approximation is.

Consider the integral expression:

$$\chi_n = \int^{\phi} (1 - n\theta\phi^n)^{1+\frac{1}{n}} d\phi. \quad (\text{B.44})$$

By expanding the structure of the correction term in this integral, the perturbation δ is given by

$$\delta = \frac{n+1}{2n^2\theta} (A_n^{-n} \chi^{-\frac{n}{n+2}}). \quad (\text{B.45})$$

In this case, the potential can be written as

$$V(\chi_n) = V_0(\chi_n) \tilde{\delta}, \quad (\text{B.46})$$

where

$$\tilde{\delta} = 1 + K\delta \quad (\text{B.47})$$

with

$$K = \frac{m}{1 - n\theta A_n^n \chi_n^{n/(n+2)}}. \quad (\text{B.48})$$

This leads to the following decomposition for the logarithm of the potential:

$$\log V = \log V_0 + \log \tilde{\delta}. \quad (\text{B.49})$$

The resulting corrections to the slow-roll parameters can then be evaluated as

$$\Delta\epsilon_V = M_{pl}^2 \left(\frac{\partial}{\partial\chi} \log V_0 \right) \left(\frac{\partial}{\partial\chi_n} \ln \tilde{\delta} \right), \quad (\text{B.50})$$

$$\Delta\eta_V = 2M_{pl}^2 \left(\frac{\partial}{\partial\chi} \log V_0 \right) \left(\frac{\partial}{\partial\chi_n} \ln \tilde{\delta} \right) + M_{pl}^2 \frac{\partial^2}{\partial\chi_n^2} \ln \tilde{\delta}. \quad (\text{B.51})$$

Using these expressions, the corrections to the observable quantities can be estimated as

$$\Delta n_s \approx -6\Delta\epsilon_V + 2\Delta\eta_V, \quad (\text{B.52})$$

$$\Delta r \approx 16\Delta\epsilon_V. \quad (\text{B.53})$$

When $\delta \ll 1$, these corrections provide a sufficiently accurate approximation while neglecting higher-order terms. Therefore, δ serves as one of the primary indicators of theoretical uncertainty in the model predictions.

C Validity Range of the Squeezing Parameter θ

We estimate the valid range of the Virasoro–squeezing parameter θ and discuss its relation to the observed quantities (A_s, r) . This appendix provides a quantitative justification for the natural interval of θ constrained simultaneously by observational data and regularity (absence of branch singularities).

C.1 Slow-roll approximation and curvature power spectrum

Under the slow-roll approximation, the Hubble parameter H and the potential $V(\phi)$ satisfy

$$3M_{pl}^2 H^2 \simeq V, \quad (\text{C.1})$$

$$3H\dot{\phi} \simeq -V'. \quad (\text{C.2})$$

The slow-roll parameters are defined as

$$\epsilon_V = \frac{M_{pl}^2}{2} \left(\frac{V'}{V} \right)^2, \quad \epsilon_H = -\frac{\dot{H}}{H^2} \simeq \epsilon_V. \quad (\text{C.3})$$

The tensor-to-scalar ratio is then given by

$$r = 16\epsilon_H c_s \simeq 16\epsilon_V c_s, \quad (\text{C.4})$$

where c_s denotes the sound speed of scalar perturbations.

The power spectrum of curvature perturbations is expressed as

$$\mathcal{P}_{\mathcal{R}}(k) = \frac{H^2}{8\pi^2 M_{pl}^2 \epsilon_H c_s} \simeq \frac{V}{24\pi^2 M_{pl}^4 \epsilon_V c_s}. \quad (\text{C.5})$$

At the pivot scale $k_0 = 0.002 \text{ Mpc}^{-1}$ (Planck 2018 convention), the observed quantities are

$$A_s \equiv \mathcal{P}_{\mathcal{R}}(k_0) \simeq 2.1 \times 10^{-9}, \quad r(k_0) \lesssim 0.03. \quad (\text{C.6})$$

C.2 Virasoro–squeezed potential and plateau height

The Virasoro–squeezed potential is given by

$$V_\chi(\chi) = V(|F_n(\phi(\chi))|^2), \quad F_n(\phi(\chi)) = \frac{\phi(\chi)}{(1 - n\theta\phi(\chi)^n)^{1/n}}. \quad (\text{C.7})$$

From the maximum–modulus principle (no local extrema inside the regular domain) and the asymptotic behavior of F_n , one obtains

$$|F_n(\phi(\chi))| \xrightarrow{|\phi| \rightarrow \infty} |n\theta|^{-1/n}. \quad (\text{C.8})$$

Thus, an m -th order potential takes the plateau form during slow roll:

$$V(\chi) = \frac{\lambda_m}{m} |F_n(\phi(\chi))|^m \approx \frac{\lambda_m}{m} |n\theta|^{-m/n}. \quad (\text{C.9})$$

C.3 Relation to the observed quantities

Using the expression for A_s ,

$$A_s = \frac{V}{24\pi^2 M_{\text{pl}}^4 \epsilon_V c_s} \simeq \frac{V}{24\pi^2 M_{\text{pl}}^4 r c_s / 16} = \frac{2}{3} \frac{\pi^2 V}{M_{\text{pl}}^4 c_s} \frac{1}{r}. \quad (\text{C.10})$$

At the pivot scale, the corresponding plateau potential is

$$V_{\text{pl}} = \frac{3}{2} \pi^2 A_s r M_{\text{pl}}^4 c_s. \quad (\text{C.11})$$

Equating this with the plateau height of the Virasoro–squeezed potential gives

$$\frac{\lambda_m}{m} |n\theta|^{-m/n} = \frac{3}{2} \pi^2 A_s r M_{\text{pl}}^4 c_s, \quad (\text{C.12})$$

which yields

$$|n\theta|^{-\frac{m}{n}} = \frac{3}{2} \pi^2 \frac{m}{\lambda_m} A_s r M_{\text{pl}}^4 c_s. \quad (\text{C.13})$$

Hence,

$$\boxed{|\theta| = \frac{1}{|n|} \left(\frac{\lambda_m}{m} \right)^{\frac{n}{m}} \left(\frac{3}{2} \pi^2 A_s r M_{\text{pl}}^4 c_s \right)^{-\frac{n}{m}}}. \quad (\text{C.14})$$

C.4 Scaling relations

From the above expression, the scaling of the squeezing parameter is

$$|\theta| \propto r^{-\frac{n}{m}}, \quad |\theta| \propto A_s^{-\frac{n}{m}}. \quad (\text{C.15})$$

For example, for $m = 2$:

$$n = -2: |\theta| \propto r^{+1}, A_s^{+1}, \quad n > 0: |\theta| \propto r^{-n/2}. \quad (\text{C.16})$$

Thus, for $n = -2$, a larger r leads to a larger $|\theta|$, whereas for $n > 0$, smaller r requires larger $|\theta|$.

C.5 Regularity constraint and sign of θ

Since F_n has a branch point at

$$\phi_c = |(n\theta)^{-1/n}|, \quad (\text{C.17})$$

the field value at the end of inflation ϕ_{end} (defined by $\epsilon_V(\phi_{\text{end}}) = 1$) must lie inside the regular domain:

$$|\phi_{\text{end}}| < |\phi_c|. \quad (\text{C.18})$$

This gives the upper bound

$$\boxed{|\theta| < \frac{|\phi_{\text{end}}|^{-n}}{|n|}}. \quad (\text{C.19})$$

The sign of θ is fixed by regularity along the real axis:

$$\boxed{n > 0 \Rightarrow \theta < 0, \quad n < 0 \Rightarrow \theta > 0}. \quad (\text{C.20})$$

C.6 Summary

The squeezing parameter θ is therefore constrained by two independent conditions:

1. Observational constraint

$$|\theta| = \frac{1}{|n|} \left(\frac{\lambda_m}{m} \right)^{\frac{n}{m}} \left(\frac{3}{2} \pi^2 A_s r M_{\text{pl}}^4 c_s \right)^{-\frac{n}{m}}. \quad (\text{C.21})$$

2. Regularity constraint

$$|\theta| < \frac{|\phi_{\text{end}}|^{-n}}{|n|}. \quad (\text{C.22})$$

When these conditions are satisfied simultaneously—together with the sign rule above—the parameter θ acquires a natural and non-arbitrary range determined entirely by the observational quantities (A_s, r) and by the mathematical requirement of analyticity of the Virasoro-squeezed transformation.

References

- [1] Planck Collaboration. Planck2018 results: I. overview and the cosmological legacy of planck. *Astronomy and Astrophysics*, 641:A1, September 2020.
- [2] BICEP/Keck Collaboration. Improved constraints on primordial gravitational waves using planck, wmap, and bicep/ keck observations through the 2018 observing season. *Physical Review Letters*, 127(15):151301, October 2021.
- [3] Wayne Hu and Scott Dodelson. Cosmic microwave background anisotropies. *Annual Review of Astronomy and Astrophysics*, 40(1):171–216, September 2002.
- [4] A.A. Starobinsky. A new type of isotropic cosmological models without singularity. *Physics Letters B*, 91(1):99–102, March 1980.
- [5] A.D. Linde. Chaotic inflation. *Physics Letters B*, 129(3–4):177–181, September 1983.
- [6] Alexandros Kehagias, Azadeh Moradinezhad Dizgah, and Antonio Riotto. Remarks on the starobinsky model of inflation and its descendants. *Physical Review D*, 89(4):043527, February 2014.
- [7] Renata Kallosh and Andrei Linde. Hybrid cosmological attractors. *Physical Review D*, 106(2):023522, July 2022.
- [8] Eva Silverstein and Alexander Westphal. Monodromy in the cmb: Gravity waves and string inflation. *Physical Review D*, 78(10):106003, November 2008.
- [9] Shamit Kachru, Renata Kallosh, Andrei Linde, Juan Maldacena, Liam McAllister, and Sandip P Trivedi. Towards inflation in string theory. *Journal of Cosmology and Astroparticle Physics*, 2003(10):013–013, October 2003.
- [10] Renata Kallosh and Andrei Linde. On the present status of inflationary cosmology. 2025.

- [11] Renata Kallosh and Andrei Linde. Universality class in conformal inflation. *Journal of Cosmology and Astroparticle Physics*, 2013(07):002–002, July 2013.
- [12] Kei-ichiro Kubota, Hiroki Matsui, and Takahiro Terada. Inflationary α -attractor models with singular derivative of potential. *Journal of Cosmology and Astroparticle Physics*, 2023(07):011, July 2023.
- [13] Sukannya Bhattacharya, Koushik Dutta, Mayukh R. Gangopadhyay, and Anshuman Maharana. α -attractor inflation: Models and predictions. *Physical Review D*, 107(10):103530, May 2023.
- [14] Laura Iacconi, Matteo Fasiello, Jussi Väliviita, and David Wands. Novel cmb constraints on the α parameter in alpha-attractor models. *Journal of Cosmology and Astroparticle Physics*, 2023(10):015, October 2023.
- [15] So Katagiri, Akio Sugamoto, Koichiro Yamaguchi, and Tsukasa Yumibayashi. Beyond squeezing à la virasoro algebra. *Progress of Theoretical and Experimental Physics*, 2019(12), December 2019.
- [16] So Katagiri. Unlocking novel quantum states: Virasoro-bogoliubov transformations in two modes. *arXiv preprint arXiv:2312.07247*, 2023.
- [17] Huber Nieto-Chaupis. Canonical commutation relation derived from witt algebra. *Mathematics*, 13(12):1910, June 2025.
- [18] Lars Valerian Ahlfors. *Complex analysis*. McGraw Hill, third edition edition, 1979.
- [19] David Wands, Nicola Bartolo, Sabino Matarrese, and Antonio Riotto. Observational test of two-field inflation. *Physical Review D*, 66(4):043520, August 2002.